### Title

PERIOD phosphorylation leads to feedback inhibition of CK1 activity to control circadian period




### Journal

Molecular Cell, 83(10)

### ISSN

1097-2765



### Authors

Philpott, Jonathan M

Freeberg, Alfred M

Park, Jiyoung

et al.



### Publication Date

2023-05-01

### DOI

10.1016/j.molcel.2023.04.019

Peer reviewed

HHS Public Access

Author manuscript

*Mol Cell*. Author manuscript; available in PMC 2024 December 30.

Published in final edited form as:

*Mol Cell*. 2023 May 18; 83(10): 1677–1692.e8. doi:10.1016/j.molcel.2023.04.019.

# PERIOD phosphorylation leads to feedback inhibition of CK1 activity to control circadian period

**Jonathan M. Philpott**[1], **Alfred M. Freeberg**[1], **Jiyoung Park**[2], **Kwangjun Lee**[2], **Clarisse G. Ricci**[3,‡], **Sabrina R. Hunt**[1], **Rajesh Narasimamurthy**[4], **David H. Segal**[1], **Rafael Robles**[1], **Yao Cai**[5], **Sarvind Tripathi**[1], **J. Andrew McCammon**[3,6], **David M. Virshup**[4,7], **Joanna C. Chiu**[5], **Choogon Lee**[2,*], **Carrie L. Partch**[1,8,9,*]

[1]Department of Chemistry and Biochemistry, University of California Santa Cruz, Santa Cruz, CA 95064

[2]Department of Biomedical Sciences, College of Medicine, Florida State University, Tallahassee, FL 32306

[3]Department of Chemistry and Biochemistry, University of California San Diego, La Jolla, CA 92093

[4]Program in Cancer and Stem Cell Biology, Duke-NUS Medical School, Singapore,169857

[5]Department of Entomology and Nematology, University of California Davis, Davis, CA 95616

[6]Department of Pharmacology, University of California San Diego, La Jolla, CA 92093

[7]Department of Pediatrics, Duke University Medical Center, Durham, NC 27710

[8]Center for Circadian Biology, University of California San Diego, La Jolla, CA 92093

[9]Lead contact

## Summary

PERIOD (PER) and Casein Kinase 1δ regulate circadian rhythms through a phosphoswitch that controls PER stability and repressive activity in the molecular clock. CK1δ phosphorylation of the Familial Advanced Sleep Phase (FASP) serine cluster embedded within the Casein Kinase 1 binding domain (CK1BD) of mammalian PER1/2 inhibits its activity on phosphodegrons to stabilize PER and extend circadian period. Here, we show that the phosphorylated FASP region (pFASP) of PER2 directly interacts with and inhibits CK1δ. Co-crystal structures in conjunction with accelerated molecular dynamics simulations reveal how pFASP phosphoserines dock into conserved anion binding sites near the active site of CK1δ. Limiting phosphorylation of the

*Correspondence: cpartch@ucsc.edu, choogon.lee@med.fsu.edu.
‡Current address: D.E. Shaw Research, New York, NY 10036

Author contributions

Conceptualization: J.M.P., S.R.H., C.L., and C.L.P.; Software: C.G.R. and J.A.M.; Investigation: J.M.P., A.F.M., J.P., K.L., S.R.H., R.N., D.H.S., R.R., and J.C.C.; Formal Analysis: J.M.P., A.M.F., S.R.H., R.N., Y.C., and S.T.; Writing – Original draft: J.M.P., C.G.R., C.L., and C.L.P.; Writing – Review & Editing: J.M.P., C.G.R., R.N., D.M.V., J.C.C., C.L., and C.L.P.; Visualization: J.M.P.; Supervision: J.A.M., D.M.V., J.C.C., C.L., and C.L.P.; Project Administration: C.L. and C.L.P.; Funding Acquisition: J.A.M., D.M.V., J.C.C., C.L., and C.L.P.

Declaration of interests

The authors declare no competing interests.

FASP serine cluster reduces product inhibition, decreasing PER2 stability and shortening circadian period in human cells. We found that *Drosophila* PER also regulates CK1δ via feedback inhibition through the phosphorylated PER-Short domain, revealing a conserved mechanism by which PER phosphorylation near the CK1BD regulates CK1 kinase activity.

## Introduction

The mammalian circadian clock is driven by a set of interlocked transcription-translation feedback loops (Takahashi, 2017). The core feedback loop is driven by the heterodimeric transcription factor, CLOCK:BMAL1, that promotes the transcription of multiple clock-controlled genes including its own repressors, Period (PER) and Cryptochrome (CRY) (Koike et al., 2012). PER proteins nucleate formation of a complex with CRYs and the clock-associated kinase, Casein Kinase 1 δ/ε (CK1) (Aryal et al., 2017; Lee et al., 2001; Michael et al., 2017) that ultimately bind to and inhibit CLOCK:BMAL1 activity (Cao et al., 2021), so the relative abundance of PER proteins is tightly regulated (Chen et al., 2009; Lee et al., 2011b) by transcriptional, post-transcriptional, and post-translational mechanisms (Crosby and Partch, 2020). The abundance of PER proteins is critical, as constitutive overexpression of PER proteins disrupts circadian rhythms (Chen *et al.*, 2009) while the inducible regulation of PER expression on a daily basis can establish circadian rhythms *de novo* with tunable periods (D'Alessandro et al., 2015).

The post-translational control of PER stability by its cognate kinase, CK1, has been widely studied. CK1 remains stably bound, or anchored, to PER1 and PER2 throughout the circadian cycle (An et al., 2022; Aryal *et al.*, 2017; Lee *et al.*, 2001) via a conserved Casein Kinase 1 Binding Domain (CK1BD) (Eide et al., 2005; Lee et al., 2004). CK1 regulates PER2 stability through a phosphoswitch mechanism, whereby the anchored kinase phosphorylates antagonistic sites on PER2 that, on balance, control its stability (Zhou et al., 2015). CK1 phosphorylation of a Degron located several hundred residues upstream of the CK1BD, near the tandem PAS domains of PER2, leads to recruitment of the E3 ubiquitin ligase, β-TrCP, and subsequent proteasomal degradation (Eide *et al.*, 2005; Masuda et al., 2020; Ohsaki et al., 2008; Vanselow et al., 2006). Activity at this PAS-Degron is counteracted somehow by CK1-dependent phosphorylation of a multi-serine cluster within the CK1BD known as the FASP region. This region is named for a Ser to Gly polymorphism in human *Per2* (S662G) that disrupts CK1 activity at this cluster (Narasimamurthy et al., 2018), destabilizing PER2 and shortening circadian period, leading to Familial Advanced Sleep Phase Syndrome (Toh et al., 2001) that impacts the timing of sleep onset in humans (Jones et al., 2013). Mutations in CK1 can also alter the balance of its activity on these two regions to significantly shorten circadian period *in vivo* (Lowrey et al., 2000; Xu et al., 2005; Xu et al., 2007).

Similar to the FASP region of mammalian PER1/2, phosphorylation of the PER-Short domain of *Drosophila* PER (dPER) by DOUBLETIME (DBT, the *Drosophila* homolog of CK1δ/ε) and NEMO/NLK attenuates DBT-dependent phosphorylation at an N-terminal Degron to stabilize dPER and regulate circadian period (Chiu et al., 2011; Chiu et al., 2008). In particular, DBT-dependent phosphorylation of S589, the site of the classic $per^S$ mutation

(S589N) within the PER-Short domain (Konopka and Benzer, 1971), stabilizes PER in its inhibition-active form while mutation of this residue is sufficient to destabilize PER and shorten circadian period (Top et al., 2018). Phosphorylation of S596 by the NEMO/NLK kinase is required for DBT-dependent phosphorylation of nearby sites within the PER-Short domain, including S589, suggesting a hierarchical phosphorylation program that acts as a time-delay in the regulation of dPER abundance and repressive activity (Chiu *et al.*, 2011).

In this study, we discovered how CK1 phosphorylation of the stabilizing FASP or PER-Short domains leads to feedback inhibition of the kinase. First, we found that multisite phosphorylation of the human PER2 FASP region is gated by rate-limiting phosphorylation of the first of five sequential serines in the FASP cluster by CK1. After this slow priming, CK1 rapidly phosphorylates the remaining serines in the FASP cluster following an ordered-distributive kinetic mechanism. Phosphorylation of C-terminal sites within the FASP region leads to product inhibition of CK1, reducing the overall rate of priming phosphorylation. Consistent with this, we show that phosphorylated FASP (pFASP) peptides inhibit CK1 activity on the PAS-Degron *in vitro.* Crystal structures and molecular dynamics simulations of the pFASP-bound kinase reveal the mechanism of product inhibition, driven by the interaction between pFASP and highly conserved anion binding sites on CK1. Leveraging newly developed U2OS $PER1^{Luc}$ and $PER2^{Luc}$ reporter cell lines (Park, 2022), we used CRISPR-generated indels to disrupt phosphorylation within the FASP region of *Per1* or *Per2*, observing shorter circadian periods and demonstrating conservation of the pFASP phosphoswitch in PER1 and PER2. Likewise, we discovered that phosphorylation of the PER-Short domain of *Drosophila* PER, located just upstream of the CK1BD, also inhibits CK1 activity *in vitro.* A structure of CK1 bound to a PER-Short domain phosphopeptide reveals a similar mechanism of product inhibition. Taken together, these results establish a conserved mechanism by which CK1 activity is regulated by feedback inhibition of PER to control PER stability and kinase activity within the molecular clock.

## Results

### CK1 phosphorylates the serine cluster in the PER2 FASP region in a sequential manner

The FASP region is an intrinsically disordered stretch of ~50 highly conserved residues embedded within the CK1BD of PER1 and PER2 that contains a cluster of 5 serine residues with the repeated spacing of SxxS (Figure 1a). We previously showed that CK1 is necessary and sufficient to initiate phosphorylation of the FASP region in mouse PER2 by targeting the first serine within this cluster in a rate-limiting step known as priming (Narasimamurthy *et al.*, 2018). We sought to extend this analysis to study the mechanism of multisite phosphorylation within the intact human PER2 FASP region using an NMR-based kinase assay that provides site-specific resolution of kinase activity on an $^{15}$N-labeled peptide substrate (Narasimamurthy *et al.*, 2018; Smith et al., 2015). Using a constitutively active version of CK1δ lacking its autoinhibitory C-terminal tail, we found that CK1 phosphorylated all 5 serines within the FASP region (Figure 1b, Supplementary Figure 1a). Based on the CK1 consensus recognition motif, pSxxS (Flotow et al., 1990), we expected that CK1 would phosphorylate serines downstream of the priming site in a sequential manner. To test this, we introduced alanine mutations at each successive serine

within the FASP cluster and assayed CK1 activity in the NMR kinase assay (Figure 1c–f). As expected, each Ser/Ala substitution selectively disrupted CK1 activity at downstream serines, confirming that the kinase acts in a sequential manner and generating a set of variably phosphorylated FASP peptides to study the functional consequences of kinase activity on this region.

### CK1 follows an ordered distributive mechanism gated by slow, non-consensus priming

Due to the sequential nature of FASP phosphorylation by CK1, we propose that the kinase follows an ordered distributed kinetic mechanism (Figure 2a). The transient accumulation of intermediates can theoretically be observed by NMR, depending on the rate constants for intermediate states (Figure 2b–c) (Cordier et al., 2012). Since we previously determined that phosphorylation of the non-consensus priming serine was much slower than consensus-based activity on subsequent serines (Narasimamurthy *et al.*, 2018), we expected that phosphorylation of the FASP would appear to be an all-or-none event by NMR, represented by state F in Figure 2b. When phosphorylation sites are in close proximity to one another, the chemical shift of a particular residue can change over the course of a reaction as nearby sites become modified (Smith *et al.*, 2015). Using the distinct phosphospecies generated with alanine substitutions in the FASP, we were able to assign unique chemical shifts for each phosphopeak that arises as a function of sequential phosphorylation (Supplementary Figure 1b). However, in a kinase reaction with the native FASP, we did not observe accumulation of any intermediate states over the course of the reaction, only a set of peaks corresponding to the 5 phosphoserines defined as species C in Figure 2d and e. We did observe a second slow step due to phosphorylation of T675 (peak 6D in Figure 2d) that was dependent on phosphorylation of the upstream residue S671 (Supplementary Figure 1b), consistent with the less optimal CK1 consensus motif of pSxxxS/T (Flotow *et al.*, 1990). The peaks corresponding to phosphoserines 4 and 5 (pS671 and pS674) were split depending on whether or not T675 was phosphorylated (4C and 4D, 5C and 5D, Figure 2d).

We confirmed the overall kinetic scheme by collecting a series of 6-minute SoFast HMQC (heteronuclear multiple-quantum correlation) NMR spectra over the course of a 3-hr real-time kinase reaction in the magnet (Figure 2f). Combining the total intensities for phosphoserines 4 and 5 from states C and D (Figure 2g) confirms that the reaction kinetics proceed as predicted by the model outlined in Figure 2b. To probe the ordered distributive mechanism, we utilized a mutant form of the kinase, K224D (Shinohara et al., 2017), that disrupts the anion binding pocket Site 1 near the active site thought to anchor primed substrates and facilitate kinase activity on downstream consensus sites (Longenecker et al., 1996; Venkatesan et al., 2019; Zeringo and Bellizzi, 2014). The K224D mutant retains its ability to prime the FASP region with kinetics similar to the WT kinase but has decreased activity on subsequent consensus-based sites (Philpott et al., 2020). By reducing the relative difference in rates for priming and sequential phosphorylation with this mutant, we were able to resolve a distinct peak corresponding to the transient accumulation of the primed, singly phosphorylated FASP, like that observed in the PER2 S665A mutant (Figure 2h), which exhibited a clear lagging phase for kinase activity on subsequent phosphorylation sites (Figure 2i). These results confirmed a distributive model of product release and

rebinding, whereas if the mechanism were processive we should have only seen one chemical shift for each serine in the final phosphorylated species.

Mutation of the priming serine in the human FASP region to an aspartate, S662D, rescues downstream kinase activity within the FASP region (Toh *et al.*, 2001) and increases circadian period by promoting the stabilization of PER2 in mice (Xu *et al.*, 2007). Other CK1 substrates are constitutively primed by D/E residues upstream that can act as phosphomimetics (Flotow and Roach, 1991; Marin et al., 2003). Using the NMR kinase assay, we observed that while the S662D mutation can prime kinase activity on downstream serines within the FASP region, it is a relatively poor mimetic of pS662, leading to a reduction in the overall kinase activity on the FASP peptide (Supplementary Figure 1c–d). Therefore, the ability of the S662D mutant to promote PER2 stability and period lengthening *in vivo* (Xu *et al.*, 2007) likely rests on the weak but constitutive priming of downstream serines by the aspartate.

## Sequential phosphorylation of FASP leads to feedback inhibition of CK1

Disrupting phosphorylation of the FASP region by mutating the priming serine increases CK1 activity at a phosphodegron in PER2 (Philpott *et al.*, 2020), consistent with increased PER2 turnover in the human FASPS S662G mutant (Toh *et al.*, 2001). However, no mechanistic model has been robustly demonstrated yet for how FASP phosphorylation influences CK1 activity. Monitoring both the loss of peak intensity for S662 and the concomitant increase in peak intensity for pS662, we made the striking observation that the fraction of primed WT FASP plateaued at approximately 50% completion over the course of a 3-hr real-time NMR kinase assay (Figure 3a). This suggested to us that some or all of the phosphoserines in the FASP cluster might work to reduce CK1 activity via feedback inhibition. To dissect the role of successive phosphoserines in this inhibition, we monitored the kinetics of FASP priming by NMR using the alanine-substituted mutants that limit the extent of sequential phosphorylation in a stepwise manner (Figure 3b–e). We found that reducing the extent of possible phosphosites in the FASP led to a stepwise increase in priming activity, resulting in near complete priming of the S668A mutant that was limited to just 2 phosphoserines (Figure 3d) and a several-fold increase in the rate of priming ($k_{prime}$) relative to the WT FASP (Figure 3f).

To confirm that the observed inhibition of FASP priming was due to feedback inhibition, we performed substrate titration experiments using an ADP-Glo assay that measures bulk kinase activity. Here, we observed that WT FASP had the lowest overall rate of phosphorylation, despite having the most consensus-based phosphosites available for the kinase (Figure 3e,g). Moreover, kinase activity began to decrease on WT FASP at higher substrate concentrations, consistent with substrate/product inhibition. As in the NMR based assay, we observed a rank-order increase in overall kinase activity and decrease in apparent inhibition as the extent of possible phosphosites in FASP was successively limited with the alanine substitutions (Figure 3g), shifting the Michaelis constant higher for each of these peptides (Figure 3h, Supplementary Figure 2a). Together, these data are consistent with the rapid generation of a pFASP product that inhibits kinase activity in *trans*. To test this, we performed a kinase assay on a peptide corresponding to the PAS-Degron

of PER2 (Supplementary Figure 2b) (Isojima et al., 2009) in the presence or absence of synthetically phosphorylated FASP peptides (pFASP) with varying levels of phosphorylation and truncated to remove any downstream phosphorylation sites. The doubly phosphorylated FASP peptide (2pFASP) inhibited the kinase in *trans*, with the 3pFASP peptide further increasing the potency of inhibition (Figure 3i). Addition of the 4pFASP peptide in *trans* also inhibited phosphorylation of the priming serine in an *in vitro* kinase assay, where full-length mouse PER2 expressed and immunoprecipitated from HEK293 cells was treated with CK1δ kinase pre-incubated with 4pFASP peptide (Figure 3j–k).

We performed real-time bioluminescence measurements of HEK293T cells transiently transfected with hPER2::LUC and CK1δ expression plasmids to monitor the half-life of hPER2::LUC in the context of Ser/Ala mutations that modulate PER2 phosphorylation. Consistent with prior results, mutation of the PAS-Degron site (S480) to an alanine increased hPER2::LUC stability (Supplementary Figure 2c), where S480 corresponds to the first phosphorylated residue of the β-TrCP consensus recognition motif, DpSGYGpS (Supplementary Figure 2b) (Eide *et al.*, 2005; Reischl et al., 2007; Wu et al., 2003). Mutation of either the priming serine (S662A) or downstream serines (i.e., S671A or S674A) decreased PER2::LUC half-life, while mutation of the threonine residue at the end of the FASP cluster (T675A) showed no significant effect on PER2 stability (Supplementary Figure 2c). To further link the Ser/Ala mutations in FASP to β-TrCP recognition of PER2, we performed co-immunoprecipitation experiments from HEK293T cells co-transfected with PER2, β-TrCP and CK1δ expression plasmids and observed increased CK1δ-dependent β-TrCP binding to PER2 with mutants that reduce FASP phosphorylation (Supplementary Figure 2d–e).

## pFASP binds to CK1 via conserved anion binding sites to occlude the substrate binding cleft

CK1 has several highly conserved anion binding sites located around the substrate binding cleft (Figure 4a) (Longenecker *et al.*, 1996; Philpott *et al.*, 2020). Given their location and the distance between phosphosites within pFASP, we hypothesized that these anion binding sites might mediate interaction of the phosphorylated peptide with CK1. Moreover, crystal structures of CK1δ in complex with phosphorylated substrates of p63 have recently been shown to interact with these anion binding sites (Gebel et al., 2020). To test whether the phosphorylated FASP region could interact with these anion binding sites in a similar manner, we solved crystal structures of phosphorylated FASP peptides bound to the catalytic domain of CK1δ (Table 1). Indeed, in three distinct complexes with 2pFASP, 3pFASP, or 4pFASP peptides, we observed a consistent binding mode (Supplementary Figure 3a) with the phosphorylated peptides coordinating the two anion binding sites (Site 1 and Site 2) to fully occlude the substrate binding cleft (Figure 4b). Interestingly, a substrate motif analysis derived from a dataset of 101 known CK1δ substrate sequences from PhosphoSitePlus aligns well with this pFASP binding mode, suggesting that the first 3 sites of the FASP region conform to an ideal CK1δ recognition sequence (Supplementary Figure 3b). The binding mode of pFASP and phosphorylated p63 peptides is largely similar (Supplementary Figure 4c), suggesting that product inhibition of CK1 activity is a conserved mechanism in these systems. In Site 1, R178 and the backbone amide of G215 coordinate pS662 of the

pFASP peptide (Figure 4c). Site 1 harbors the location of the *tau* mutation (R178C) that shortens circadian period (Lowrey *et al.*, 2000). We did not observe strong density for K224, the other basic residue that could coordinate an anion in Site 1, suggesting flexibility in the Fα helix observed in previous studies (Cullati et al., 2022; Philpott *et al.*, 2020; Shinohara *et al.*, 2017). Moving down the pFASP peptide, we observed additional backbone-backbone interactions and docking of the pFASP side chains of V663 & A664 into small hydrophobic pockets within the substrate binding cleft (Figure 4b, d).

The 2$^{nd}$ phosphoserine of pFASP, pS665, projected into the active site of CK1, positioned close to where the gamma phosphate would be in ATP-bound CK1 (Supplementary Figure 3c). We also observed that S19 of the N-terminal lobe P-loop of CK1 clamped down on pS665, suggesting a stabilizing mechanism for transfer of phosphate from the nucleotide to the substrate, with the +1 Leu after pS665 fitting into a small hydrophobic pocket on the kinase. As previously noted, this small hydrophobic pocket is formed between L173 and Y225 of CK1 (the +1 pocket, Figure 4b, d) in the downward conformation of the CK1 activation loop (Philpott *et al.*, 2020). The +1 pocket is just large enough to accommodate small residues such as Ala, Leu, or Val, and could contribute to CK1 recognition of the non-consensus SLS motif (Marin *et al.*, 2003) or the FASP priming site, where the +1 residue is a valine. In complexes with phosphorylated p63 peptides, the 2$^{nd}$ phosphoserine has a +1 polar Thr residue that perhaps prevents this residue from coordinating the active site like the 2$^{nd}$ phosphoserine of pFASP. This difference in amino acid sequence between the p63 and pFASP peptides could contribute to the overall difference in binding modes between the peptides, with leaving Site 2 of the kinase unoccupied by phosphoserines in the p63 peptides.

Moving towards the C-terminal end of the peptide, the 3$^{rd}$ phosphoserine of pFASP, pS668, is coordinated by anion binding Site 2, comprising basic residues R127, K154, and K171 (Figure 4e). R127 is part of the conserved HRD motif involved in the regulation of Ser/Thr kinases by coordinating a phosphorylated residue within the activation loop (Nolen et al., 2004). To further validate the significance of these anion binding sites in the binding of pFASP and product inhibition, we introduced charge inversion mutations in Site 1 (K224D) or Site 2 (R127E) and performed substrate titrations with FASP peptide, observing a decrease in the level of product inhibition (Supplementary Figure 3d).

The highly specific sequential mechanism of FASP phosphorylation also strongly suggests that the FASP peptide translates through the substrate binding cleft, with each phosphoserine anchoring into Site 1 to facilitate the next phosphorylation event in the active site. The phosphorylated serines in pFASP all share the same approximate atomic distance between each other that is consistent with the spacing between Site 1, the active site, and Site 2. Therefore, product inhibition may continue to increase as a function of sequential phosphorylation at least partially due to changes in entropy and/or electrostatic steering, where a higher order phosphorylated FASP peptide could interact more readily with the substrate binding region of CK1 due to more favorable electrostatics and the ability to bind in multiple ways.

The *tau* mutation in Site 1 of CK1δ prevents anion coordination at this site and alters the global dynamics of CK1 as well as significantly changing the local dynamics in and around the activation loop and Site 2 via an allosteric mechanism (Philpott *et al.*, 2020). We note that the alternate conformation of the activation loop stabilized in the *tau* mutant sterically clashes with the 3pFASP binding mode (Figure 4f). This incompatibility suggests that the *tau* mutant is less susceptible to feedback product inhibition, perhaps also contributing to the increased phosphorylation of the PAS-Degron and degradation of PER2 by this kinase mutant (Gallego et al., 2006a; Philpott *et al.*, 2020; Zhou *et al.*, 2015).

## Molecular dynamics simulations support stable binding mode of pFASP:CK1 crystal structures

To investigate how CK1 might be inhibited by a fully phosphorylated FASP peptide, we modeled and simulated the interaction of CK1 and a 5pFASP peptide using Gaussian accelerated Molecular Dynamics (Supplementary Figure 4a) (details in Supplementary Material) (Miao et al., 2015). We found that the first three phosphoserines (pS662, pS665, and pS668) remain stably bound in the substrate binding cleft of CK1, while the 4$^{th}$ and 5$^{th}$ phosphoserines (pS671 and pS674) display higher mobility (Supplementary Figure 4b). As expected, pS662 forms stable electrostatic interactions in Site 1 (Figure 4g, bottom left). In addition to being close to R178 and K224, pS662 also engages in stable electrostatic interactions with Q214, located in the highly flexible loop-EF (Cullati *et al.*, 2022; Shinohara *et al.*, 2017). In the active site, pS665 is locked in place by a cluster of electrostatic interactions involving D128, K130, D148 and a $Na^+$ ion (Figure 4g, top left). The presence of this ion in the active site suggests that at least one cation (likely $Mg^{2+}$) could be important for product inhibition. The third phosphoserine (pS668) is held in place in Site 2 by stable electrostatic interactions with R127, K154, K171, and, to a lesser extent, R168 (Figure 4g, top right). Finally, we found that the 5$^{th}$ phosphoserine (pS674) often engages in electrostatic interactions with R160 (close to anion binding Site 3, which precedes the activation loop) and with K155 (just after the DFG motif) (Figure 4g, bottom right). We refer to this herein as Site 3'. These interactions provide additional product stabilization, perhaps contributing to stronger inhibition when the FASP region is fully phosphorylated.

## Substrate anchoring interactions with the PER2 CK1BD increase the phosphorylation kinetics and feedback product inhibition

Substrate anchoring/tethering interactions increase the effective concentration of substrate near the enzyme to enhance activity, although this also depends on the affinity and exchange kinetics of the anchoring interaction (Dyla et al., 2022). The CK1BD of PER1/2 is a highly conserved domain that contains two structured helical motifs (CK1BD-A/B) that flank the disordered FASP region (Figure 5a, Supplementary Figure 5a). The CK1BD facilitates the stable binding of CK1 and PER1/2 throughout their circadian cycle (An *et al.*, 2022; Aryal *et al.*, 2017; Lee *et al.*, 2001) and is essential for phosphorylation of weak, non-consensus sites on PER2 (Marzoll et al., 2022). This stable interaction between CK1 and the CK1BD of PER1/2 suggested a model where anchoring of the helical CK1BD-A/B domains acts to increase the local concentration of the FASP region near the enzyme active site (Supplementary Figure 5b). Mutation of the CK1BD-B region has been shown

to disrupt the stable anchoring interaction between CK1 and PER2 (An *et al.*, 2022) (Supplementary Figure 5c–g), preventing phosphorylation of the FASP region as well as hyperphosphorylation of PER2 in general (An *et al.*, 2022).

To examine phosphorylation of the FASP region in the context of the CK1BD, we performed an NMR kinase assay with an engineered minimal CK1BD construct (residues 571–609, 645–687, and 722–757) in a ~ 1:1 ratio with CK1 (Figure 5b). We observed the appearance of fewer phosphorylated residues, likely corresponding to the first three serines in the FASP cluster, as well as a loss of signal for residues corresponding to the rest of the residues within the FASP region upon addition of CK1. The loss of signal within the FASP region is likely due to enhanced relaxation as a result of stable interactions between the ~35 kDa CK1 kinase domain and this region in solution, further supporting our structural findings. To further compare the kinetics of FASP phosphorylation with and without anchoring interactions from the CK1BD, we performed substrate titrations with the FASP region alone or an intact CK1BD (residues 571–757). We found that anchoring in the CK1BD construct significantly increased phosphorylation kinetics of the substrate and dramatically enhanced product inhibition relative to the isolated FASP region (Figure 5c).

This suggested that stable anchoring of the kinase with the CK1BD and feedback inhibition by the phosphoFASP region could attenuate CK1 activity towards other sites on PER2, such as the Degron (Figure 5d). To test this prediction, we purified complexes of CK1 and PER2 (residues 475–757) that extend from the Degron through the CK1BD to monitor the effects of FASP phosphorylation on the Degron region *in cis* (Supplementary Figure 5h–i). We included a TEV recognition motif just downstream of the Degron (after residue 507) to cleave this region from the PER2 construct. (Supplementary Figure 5j). We monitored phosphorylation activity by mobility shift of the corresponding Degron-containing fragment in SDS-PAGE (Supplementary Figure 5j–k) and found that phosphorylation kinetics of the Degron were increased when FASP phosphorylation was disrupted by the S662G mutation (Figure 5e–f). Interestingly, we also observed a decrease in TEV cleavage efficiency over the time course that was more pronounced for the S662G mutant (Supplementary Figure 5l), suggesting that kinase activity near the Degron region may interfere with recognition of the TEV recognition sequence or its activity.

## Circadian rhythms are shortened by small deletions in the conserved FASP region of PER

To address the regulatory role of the FASP region on circadian period, small amino acid deletions were introduced in the human *Per2* FASP region encoded by exon 17 (E17) by targeting the priming serine (S662) with CRISPR (Figure 6a). This CRISPR-mediated strategy utilized human U2OS cells with endogenous *Per2-luc* and *Per1-luc* knock-in reporter genes that produced robust rhythms in bioluminescence and clock proteins (Park, 2022). As out-of-frame mutations would disrupt LUC expression and eliminate bioluminescence, we could select for small in-frame deletions in PER2::LUC protein based on intact bioluminescence signals followed by molecular characterization. Small in-frame deletions that removed the priming serine led to rhythms in PER2::LUC abundance that were phase-advanced relative to WT PER2::LUC after synchronization by serum shock

(Figure 6b). Additionally, PER1 also showed phase-advanced rhythms in abundance in these mutant lines relative to the parental cell line (Supplementary Figure 6a).

Immunoblots for priming-disrupted PER2 mutants showed similar levels of gross phosphorylation as WT PER2::LUC (Figure 6c–d, Supplementary Figure 6b). To quantify differences in period, real-time bioluminescence measurements were collected on the clonal cell lines, which exhibited robust circadian rhythms with a significantly shorter period relative to the parental cell line (Figure 6e). A comparison of the mutant genotypes suggests that the frameshift mutation in allele 2 of P2E17-3 does not significantly affect the period, whereas disruption of priming in both alleles (i.e., P2E17-50) may have an additive effect on shortening period. Mutants that left the priming serine intact but removed one or more of the downstream serines (i.e., P2E17-25) also showed robust rhythms in bioluminescence with short periods (Figure 6f, Supplementary Figure 6c), but they were not as short as the priming-disrupted mutants that eliminate all FASP phosphorylation ($P < 0.05$). This suggests a role for the downstream phosphorylation sites in regulation of CK1 activity on PER2. Disruption of the FASP region led to decreased stability of PER2 after treatment with cycloheximide (Figure 6g) and also exhibited accelerated phosphorylation kinetics relative to WT, based on mobility shift, on the *de novo* PER2 synthesized after washout of cycloheximide (Figure 6h). The FASP region is highly conserved in PER1, and similar CRISPR-mediated edits to the PER1 FASP region by targeting the priming serine S714 also exhibited short period rhythms characterized by destabilized PER1 (Supplementary Figure 6d–i). NMR studies of the human PER1 FASP demonstrate that CK1 phosphorylates it similarly to PER2 and that mutants representing the cellular indels disrupting the priming serine eliminate kinase activity on the region *in vitro* (Supplementary Figure 6j), demonstrating that the phosphorylated FASP region of both mammalian PERs likely act in a similar manner to constrain CK1 activity.

## The phosphorylated *Drosophila* PER-Short region binds CK1 to inhibit kinase activity

Mammalian and *Drosophila* PER proteins both possess the two conserved motifs comprising the CK1 binding domain (CK1BD) that stably anchors the kinase to PER throughout its daily life cycle (Eide *et al.*, 2005; Kim et al., 2007; Kivimae et al., 2008; Nawathean et al., 2007) (Supplementary Figure 7a–b). Phosphorylation of S589 on dPER by the *Drosophila* CK1 homolog DBT reduces kinase activity at a phosphodegron upstream to increase dPER stability and lengthen circadian period (Chiu *et al.*, 2011; Kivimae *et al.*, 2008) in a manner similar to the FASP-associated S662 on human PER2 (Toh *et al.*, 2001) (Supplementary Figure 7a). Loss of this phosphorylation site with the classic *per-Short* mutation (Konopka and Benzer, 1971) ($per^S$, S589N) or other mutants nearby in the PER-Short domain result in predominantly short period phenotypes (Baylies et al., 1992; Chiu *et al.*, 2011; Rothenfluh et al., 2000; Rutila et al., 1992). Because this CK1-dependent phosphosite is in close proximity to the CK1BD (Supplementary Figure 7b) (Kim *et al.*, 2007; Lee *et al.*, 2004; Nawathean *et al.*, 2007), we wondered if it would work similarly to the FASP region to attenuate CK1 activity. Phosphorylation of S589 by CK1 (i.e., DBT) has been invoked as a potential mechanism by which dPER could control CK1 activity in *trans* to regulate dPER turnover and repressive activity (Chiu *et al.*, 2011; Chiu *et al.*, 2008; Kivimae *et al.*, 2008; Top *et al.*, 2018). Phosphorylation of S589 is preceded *in vivo* by phosphorylation of S596 by

NEMO kinase, and the S596A mutation eliminates phosphorylation of S589, suggesting a hierarchical regulation of the PER-Short region by multiple kinases (Chiu *et al.*, 2011).

To determine if the phosphocluster in the PER-Short domain regulates CK1 activity on the N-terminal dPER Degron, we examined the progressive phosphorylation of this region in *Drosophila* S2 cells using a full-length dPER construct that contains a TEV-cleavable 100-residue N-terminal fragment encompassing the Degron (PER/T100) (Chiu *et al.*, 2011; Chiu *et al.*, 2008) (Supplementary Figure 7c). PER/T100 was co-expressed with full length dPER or a C-terminal fragment containing the kinase binding domain (residues 560–1034), with or without the S596A mutant, along with an inducible DBT construct. We observed that inhibition of dPER Degron phosphorylation is lost with the S596A mutant in full-length dPER (Figure 7a, c) or a fragment of dPER containing just the kinase binding domain in *trans* (Figure 7b, c). To test for direct inhibition of CK1 activity by the phosphorylated PER-Short domain, we also performed kinase assays *in vitro* using the human CK1δ kinase domain and a PER2 PAS-Degron substrate in the presence of unphosphorylated and phosphorylated dPER-Short peptides (Figure 7d). CK1 phosphorylates only S589 in this peptide *in vitro* (Kivimae *et al.*, 2008), although it is dependent upon NEMO kinase phosphorylation of S596 *in vivo* (Chiu *et al.*, 2011). Here, we observed that peptides containing pS589, pS596, or both pS589/pS596 inhibited CK1 kinase activity similarly to the 3pFASP peptide (Figure 7d).

We then sought to characterize the structural basis for this inhibition with a crystal structure of CK1 in complex with the pS589 dPER-Short domain peptide (Figure 7e–f). The CK1 and DBT catalytic domains are highly conserved and share 100% conservation within the substrate binding region (Supplementary Figure 7d). The CK1:dPER-short peptide structure revealed a binding mode similar to the pFASP, where the substrate binding cleft was largely occluded by the peptide (Figure 7e) and anchored by the coordination of pS589 at anion binding Site 1 (Figure 7f). However, the activation loop of the kinase took on the rare ‘loop up’ conformation in this complex, which disrupts the second anion binding pocket (Philpott *et al.*, 2020). This alternate conformation exposes a new channel that runs from the active site down towards the bottom of the kinase between the activation loop and helix-F that is bound by the dPER-Short peptide (Figure 7e), constricting at its narrowest point around dPER residue G593. We did not have density for residues after 595, including for pS596 in structures solved with the doubly phosphorylated peptide (data not shown). Therefore, although both mammalian and *Drosophila* PER peptides dock a critical CK1-dependent phosphoserine into anion binding Site 1, changes in peptide binding along the kinase active site suggest different mechanisms of recognition used to bind and inhibit the kinase.

## Discussion

The CK1 kinase family is defined by several highly conserved anion binding sites located around the substrate binding cleft that regulate kinase dynamics, substrate specificity, and temperature compensation of circadian rhythms (Lowrey *et al.*, 2000; Philpott *et al.*, 2020; Shinohara *et al.*, 2017). It has long been proposed these anion binding sites mediate the recruitment of phosphorylated substrates to prime activity on the CK1 consensus motif pSxxS and/or bind the autophosphorylated C-terminal tail of the kinase to inhibit its activity

(Graves and Roach, 1995; Longenecker *et al.*, 1996). Here, we show that CK1-dependent phosphorylation of key regulatory sites on its substrate PER2 near a kinase anchoring domain leads to feedback inhibition of the enzyme through these conserved anion binding sites. Anchoring interactions can significantly enhance the kinetics of kinase activity on low to moderate affinity substrates nearby (Dyla *et al.*, 2022), as was recently demonstrated for CK1 and its activity on low affinity, non-consensus phosphorylation sites on PER and FRQ (Marzoll *et al.*, 2022). Here we show that in addition to increasing kinetics on the FASP region, anchoring interactions significantly enhance feedback inhibition. Inhibition of CK1 activity by phospho-PER is conserved in both mammals and *Drosophila* through anion binding Site 1, although other details of the PER-inhibited kinase complex differ by species. Notably, the loss of these CK1-dependent phosphosites in *Drosophila* (Konopka and Benzer, 1971), mice (Xu *et al.*, 2007), and humans (Toh *et al.*, 2001) shortens circadian period by several hours *in vivo*, demonstrating the functional importance of CK1 feedback inhibition on the molecular clock.

NMR spectroscopy allowed us to probe the kinetics and mechanism of the progressive, sequential phosphorylation of the FASP region in human PER proteins by CK1. The sequential nature of kinase activity here suggests that targeting the initial, rate-limiting priming step at the FASP region could be a powerful way to influence circadian rhythms. In fact, CK1 activity here is influenced by other post-translational modifications on or around the FASP priming site, such as O-GlcNAcylation (Durgan et al., 2011; Kaasik et al., 2013) and acetylation (Levine et al., 2020), demonstrating how this region is poised to integrate different metabolic signaling inputs for control over the clock. Our data suggest that CK1 inhibition by human PER2 depends on similar spacing between successive phosphoserines on the FASP and the distance between anion coordination sites in the substrate binding region of CK1, highlighting a conserved mechanism of feedback inhibition by similar phosphorylated clusters such as found in the phosphorylation activation domain (PAD) domain of p63 (Gebel *et al.*, 2020). Although structures of inhibited CK1 illustrated a common binding mode for the first three phosphorylation sites of the FASP region, deletion of downstream sites in the U2OS *Per1* and *Per2* indel cell lines demonstrates that this region also contributes to kinase inhibition and period control, possibly as suggested by our molecular dynamics simulations.

We found that the CK1-dependent phosphoserine site in the *Drosophila* PER-Short domain, pS589, also bound to the kinase at anion binding Site 1, similar to the priming serine (pS662) of the human pFASP. However, a change in the conformation of the kinase activation loop created a new peptide binding groove that led the dPER peptide away from the active site down toward the bottom of the kinase. We could not visualize density after residue 595 in this structure, but substitutions of dPER at G593 or P597 phenocopy the $per^{S}$ mutation (S589N) (Baylies *et al.*, 1992; Konopka and Benzer, 1971), suggesting that they also contribute to binding and feedback regulation of the kinase. Furthermore, we observed that phosphorylation of S596, either alone or in combination with pS589, enhanced inhibition of CK1 by the PER-Short domain peptide *in vitro*, indicating that additional interactions between the C-terminal half of the PER-Short domain and CK1 may have been occluded by crystal packing.

Molecular mechanisms that regulate the stable association between PER and CK1, PER stability, and repressive activity appear to be broadly conserved across eukaryotes. Notably, the CK1 binding motifs are conserved in PER homologs from mammals (Eide *et al.*, 2005; Lee *et al.*, 2004), *Drosophila* (Kim *et al.*, 2007; Nawathean *et al.*, 2007) and *C. elegans* (Jeon et al., 1999), and there is functional conservation with the two helical motifs (FCD1/2) that constitute the CK1 interaction domain in *Neurospora* FRQ (He et al., 2006; Liu et al., 2019). CK1 mediates the repressive activity of PER in the mammalian clock, where CRY1/2 facilitate the recruitment of PER1/2-CK1 to the transcription factor CLOCK:BMAL1 in the nucleus, leading to its phosphorylation and displacement from DNA early in the repressive phase (Cao *et al.*, 2021; Chiou et al., 2016). Similar mechanisms of displacement-type repression are also found in *Drosophila* (Kim *et al.*, 2007) and *Neurospora* (He et al, 2006) circadian clocks. These mechanisms generally depend on CK1 activity and the strength of kinase anchoring (An *et al.*, 2022; Cao *et al.*, 2021; Liu *et al.*, 2019), although DBT catalytic activity may not be required for displacement-type repression in *Drosophila* (Yu et al., 2009). Our data suggest a model whereby phosphorylation of key regulatory sites in PER close to the CK1BD results in feedback inhibition of CK1, thereby directly regulating the ability of CK1 to phosphorylate PER and possibly other substrates within the circadian clock.

## Limitations of this study

While this study sheds light on the mechanism of pFASP product inhibition, we have not fully explored the consequences of CK1 product inhibition on regulation of circadian rhythms. In this study, we looked at inhibition of kinase activity using a PER2 substrate corresponding to the PAS-Degron; however, it is likely that feedback inhibition by a number of phosphorylated substrates such as the CK1 tail, PER2 FASP region, or dPER-Short region could differentially regulate kinase activity on other substrates as well. Previous studies have shown that CK1 autophosphorylation leads to inhibition of kinase activity *in vitro* (Cegielska et al., 1998; Graves and Roach, 1995; Rivers et al., 1998), although kinase activity seems to be largely maintained in cells via phosphatases (Rivers *et al.*, 1998). Not much is known about the regulatory roles of the CK1 tail *in vivo*, although alternate splicing of the tail generates two CK1δ isoforms that differentially regulate phosphorylation of PER2 to control circadian period (Fustin et al., 2018; Narasimamurthy *et al.*, 2018), suggesting some sort of isoform-specific regulation of CK1 activity. Recent studies have also shown that conformational changes in the CK1 catalytic domain dynamically regulate substrate selectivity (Cullati *et al.*, 2022; Philpott *et al.*, 2020), and here we show that CK1 can leverage this structural plasticity to bind different phosphorylated products with distinct binding modes. Together, these features of CK1 suggest that feedback inhibition may be a common regulatory mechanism of the kinase, but more work is needed to understand the structural and functional consequences of different inhibitory interactions.

It is not yet clear where in the cell and when in the molecular clock (i.e., the phase of the clock) that feedback regulation of CK1 activity occurs to regulate circadian rhythms. In mammals, PER1/2 form stable complexes with CRY1/2 and CK1 in the cytoplasm (Aryal *et al.*, 2017), yet PER1/2 proteins remain largely hypophosphorylated until they approach the perinucleus or after nuclear entry (Beesley et al., 2020; Lee *et al.*, 2001).

The phosphoswitch model of PER2 regulation by CK1 is consistent with this, with the longest plateaus, or pauses, in the CK1-dependent turnover of PER2 occurring early in the accumulation of PER2 (Zhou *et al.*, 2015). Ultimately, PER phosphorylation is also counterbalanced by phosphatases in mammals (Gallego et al., 2006b; Lee et al., 2011a; Schmutz et al., 2011) and *Drosophila* (Sathyanarayanan et al., 2004), so further work will be necessary to determine how kinase and phosphatase activity are integrated with other post-translational modifications to regulate PER FASP/dPER-Short phosphorylation and influence feedback regulation of CK1 activity.

## STAR Methods

### RESOURCE AVAILABILITY

**Lead contact—**Further information and requests for resources and reagents should be directed to and will be fulfilled by the lead contact, Carrie L. Partch (cpartch@ucsc.edu)

#### Materials availability

- Plasmids generated in this study are available upon request.
- U2OS reporter cell lines generated in this study are available upon request.

#### Data and code availability

- Data and code generated in this study are available upon request.
- NMR chemical shift assignments for the human FASP peptide have been deposited at BMRB and will be publicly available upon publication. BMRB entry # 51827 is listed in the Key Resources Table.
- Crystal structures of human CK1δ in complex with phosphorylated PER peptides have been deposited to the PDB and will be publicly available upon publication. Accession codes are listed in the Key Resources Table.

### EXPERIMENTAL MODEL AND SUBJECT DETAILS

#### Cell lines

- The HEK293T cell line was purchased from ATCC (#CRL-3216).
- The *Drosophila* S2 cell line was purchased from Thermo Fisher Scientific (#R69007).
- The U2OS cell line was purchased from ATCC (#HTB-96).
  - Generation of *Per* KI cell lines is described in detail in Park et al, 2022.

***Per* mutant clones in *Per*$^{Luc}$ reporter cell lines—**Heterozygous KI clones, H10 for *Per1*$^{Luc}$ and LH1 for *Per2*$^{Luc}$, were used to generate mutations in *Per1* and *Per2*, respectively. These mRuby3-expressing reporter cells were infected with all-in-one CRISPR adenovirus (*Per2*-E17-S662) or transfected with all-in-one pAdTrack-Cas9-DEST plasmids expressing GFP as described previously (Jin et al., 2019). sgRNA sequence and selected clones are summarized in the table below. For clonal isolation of mutant cells, GFP-positive

cells were sorted by FACS into 96-well plates, and these clones were further selected based on alterations in period and/or phase in bioluminescence rhythms. In each project, the majority of putative mutant clones showed a similar degree of period lengthening or shortening in bioluminescence screening. The clones used in this study were fully characterized by sequencing and immunoblotting (Supplementary File 1a.)

| Genes | Targets | sgRNA Sequences (PAMs) | Selected clones |
|---|---|---|---|
| *Per1* | Exon 17 (S714) | GGCCAATAAGGCGGAGAGTG(TGG) | *Per1*$^{Luc}$ 1, 17, 38 |
| *Per2* | Exon 17 (S662) | GCCGGGCAAGGCAGAGAGTG(TGG) | *Per2*$^{Luc}$ 17–1, 17–3, 48, 50 |
| *Per2* | Exon 17 (H678) | AGCAGCACCATCGTCCATGT(GGG) | *Per2*$^{Luc}$ 10, 25, 36 |

## METHOD DETAILS

**Expression and purification of recombinant proteins—**All proteins were expressed from a pET22-based vector in *Escherichia coli* BL21 (DE3) Rosetta2 cells (Sigma Aldrich) based on the Parallel vector series (Sheffield et al., 1999). The wild-type recombinant FASP peptide (residues 645–687) or PAS-Degron peptide (residues 475–505) were cloned from human PER2. All peptides were expressed downstream of an N-terminal TEV-cleavable His-NusA tag. Human CK1δ catalytic domains (CK1δ ΔC, residues 1–317 for kinase assays and 1–294 for crystallography) were all expressed in BL21 (DE3) Rosetta2 cells (Sigma Aldrich) with a TEV-cleavable His-GST tag. Mutations were made using standard site-directed mutagenesis protocols and validated by sequencing. All proteins and peptides expressed from Parallel vectors have an N-terminal vector artifact (GAMDPEF) remaining after TEV cleavage and the peptides have a tryptophan and polybasic motif (WRKKK) following the vector artifact. Cells were grown in LB media (for natural abundance growths) or M9 minimal media with the appropriate stable isotopes, i.e., $^{15}N/^{13}C$, for NMR as done before (Narasimamurthy *et al.*, 2018) at 37°C until the $O.D._{600}$ reached ~0.8; expression was induced with 0.5 mM IPTG, and cultures were grown for approximately 16–20 hr more at 18°C.

For CK1δ kinase domain protein preps, cells were lysed in 50 mM Tris pH 7.5, 300 mM NaCl, 1 mM TCEP, and 5% glycerol using a high-pressure extruder (Avestin) or sonicator on ice (Fisher Scientific). HisGST-CK1δ ΔC fusion proteins were purified using Glutathione Sepharose 4B resin (GE Healthcare) using standard approaches and eluted from the resin using Phosphate Buffered Saline with 25 mM reduced glutathione. His-TEV protease was added to cleave the His-GST tag from CK1δ ΔC at 4°C overnight. Cleaved CK1δ ΔC was further purified away from His-GST and His-TEV using Ni-NTA resin (Qiagen) and subsequent size exclusion chromatography on a HiLoad 16/600 Superdex 75 prep grade column (GE Healthcare) in 50 mM Tris pH 7.5, 200 mM NaCl, 5 mM BME, 1 mM EDTA, and 0.05% Tween 20. Purified CK1δ ΔC proteins used for *in vitro* kinase assays were buffer exchanged into storage buffer (50 mM Tris pH 7.5, 100 mM NaCl, 1 mM TCEP, 1 mM EDTA, and 10% glycerol) using an Amicron Ultra centrifugal filter (Millipore) and frozen as small aliquots in liquid nitrogen for storage at −80°C.

For PER2 peptide preps, cells were lysed in a buffer containing 50 mM Tris pH 7.5, 500 mM NaCl, 2 mM TCEP, 5% glycerol and 25 mM imidazole using a high-pressure extruder (Avestin) or sonicator on ice (Fisher Scientific). His-NusA-FASP or His-NusA-PAS-Degron fusion proteins were purified using Ni-NTA resin using standard approaches and eluted from the resin using 50 mM Tris pH 7.5, 500 mM NaCl, 2 mM TCEP, 5% glycerol and 250 mM imidazole. His-TEV protease was added to cleave the His-NusA tag from the PER2 peptides at 4°C overnight. The cleavage reaction was subsequently concentrated and desalted into low imidazole lysis buffer using a HiPrep 26/10 Desalting column. Peptides were purified away from His-NusA and His-TEV using Ni-NTA resin with 50 mM Tris pH 7.5, 500 mM NaCl, 2 mM TCEP, 5% glycerol and 25 mM imidazole. Peptides were purified by size exclusion chromatography on a HiLoad 16/600 Superdex 75 prep grade column, using NMR buffer (25 mM MES pH 6.0, 50 mM NaCl, 2 mM TCEP, 10 mM $MgCl_2$) or 1x kinase buffer (25 mM Tris pH 7.5, 100 mM NaCl, 10 mM $MgCl_2$, and 2 mM TCEP) for NMR or ADP-Glo kinase assays, respectively.

For CK1:PER2 complex preps, cells expressing both proteins were co-lysed in 50 mM Tris pH 7.5, 500 mM NaCl, 2 mM TCEP, and 5% glycerol. His-GST-CK1δ (1–317) and His-NusA-SUMO-Degron-CK1BD-B (475–757) were purified using Glutathione Sepharose 4B resin (GE Healthcare) using standard approaches and eluted from the resin using lysis buffer with 25 mM reduced glutathione. The His-NusA-SUMO-Degron-CK1BD-B construct contains a TEV recognition site inserted at 507. 1:1 complexes of CK1:PER2 were purified via size exclusion chromatography on a HiLoad 16/600 Superdex 200 prep grade column, using FPLC buffer (50 mM Tris pH 7.5, 200 mM NaCl, 1mM TCEP, 1mM EDTA, and 5% glycerol).

**NMR kinase assays—**NMR spectra were collected on a Varian INOVA 600 MHz or a Bruker 800 MHz spectrometer equipped with a $^{1}H$, $^{13}C$, $^{15}N$ triple resonance z-axis pulsed-field-gradient cryoprobe. Spectra were processed using NMRPipe (Delaglio et al., 1995) and analyzed using CCPNmr Analysis (Vranken et al., 2005). Backbone resonance assignments were made using standard BioPack triple resonance experiments (HNCACB, CBCA (CO)NH, HNCO, HN (CA)CO and HSQC) collected using non-uniform sampling on a sample of 0.5 mM $^{13}C$, $^{15}N$-labeled FASP in NMR buffer with 10% $D_2O$. Non-uniform sampling reconstructions were performed using software developed and provided by the Wagner lab (Delaglio *et al.*, 1995). NMR kinase reactions were performed at 25°C with 0.2 mM $^{15}N$-FASP, 2.5 mM ATP and 1 μM CK1δ ΔC (WT or K224D). SOFAST HMQC spectra (total data acquisition = 6 min) were collected at the indicated intervals for 3 hr and relative peak volumes were calculated and normalized as described previously (Narasimamurthy *et al.*, 2018). For PER1 FASP peptide kinase assays, samples were prepared as above and incubated for 2 hrs and then quenched with 20 mM EDTA and then HSQC spectra were collected. Data analysis was performed using Prism (GraphPad), with data fit to either a one-phase exponential or linear regression. For the kinase assay performed with the minimal CK1BD, 80 uM $^{15}N$-CK1BD and 60 uM CK1δ ΔC were incubated with 2.5 mM ATP at 30°C.

**Kinetic modeling—**Mathematica 11.0 (Wolfram Research) was used to model the 5-step ordered distributive kinetic model for sequential FASP phosphorylation (Figure 2a–c). Mathematica code is provided in the supplementary information (Supplementary File 1c).

**ADP-Glo kinase assays (substrate titrations)—**Kinase reactions were performed on the indicated recombinant peptides (FASP WT or Alanine mutants) using the ADP-Glo kinase assay kit (Promega) according to manufacturer's instructions. All reactions were performed in 30 μL volumes using 1x kinase buffer (25 mM Tris pH 7.5, 100 mM NaCl, 10 mM $MgCl_2$, and 2 mM TCEP) supplemented with ATP and substrate peptides. To determine apparent kinetic parameters $K_M$ and $V_{max}$, duplicate reactions with 100 μM ATP and 0.2 μM CK1δ ΔC kinase were incubated in 1x kinase buffer at room temperature for 1 hr with the indicated amount of substrate peptide (and repeated for n = 3 independent assays). 5 μL aliquots were taken and quenched with ADP-Glo reagent after the 1 hr incubation, and Luminescence measurements were taken at room temperature with a SYNERGY2 microplate reader (BioTek) in 384-well microplates. Linearity of the 1 hr reaction rate was determined by performing larger reactions (50 μL) with CK1δ ΔC and quenching at discrete time points (data not shown). Data analysis was performed using Excel (Microsoft) or Prism (GraphPad).

**ADP-Glo kinase assays (peptide inhibition)—**Kinase reactions were performed on the recombinant PAS-Degron peptide (Supplementary Figure 2b) using the ADP-Glo kinase assay kit (Promega) according to manufacturer's instructions. Synthetic peptide inhibitors were solubilized in 1x kinase buffer (25mM Tris pH 7.5, 100 mM NaCl, 10 mM $MgCl_2$, and 2 mM TCEP) at a concentration of 10 mM. All kinase reactions were performed in 30 μL reactions supplemented with ATP, PAS-Degron substrate, and synthetic peptide inhibitors. Duplicate reactions (repeated for n = 3 independent assays) with 100 μM ATP, 0.2 μM CK1δ ΔC kinase, and 100 μM PAS-Degron substrate were incubated in 1x kinase buffer at room temperature for 1 hr in the presence of increasing amounts of synthetic peptide inhibitors (phosphorylated FASP or dPER peptides) as indicated. 5 μL aliquots were quenched with ADP-Glo reagent after the 1 hr incubation, and luminescence measurements were taken at room temperature with a SYNERGY2 microplate reader (BioTek) in 384-well microplates. Data analysis was performed using Excel (Microsoft) or Prism (GraphPad).

**Full-length PER2 kinase assay (peptide inhibition)—**HEK293 cells transfected with Myc-PER2 plasmid were lysed in cell lysis buffer (50 mM Tris-HCl pH 8.0, 150 mM NaCl, 1% Nonidet P-40, and 0.5% deoxycholic acid containing Complete protease inhibitors (Roche) and PhosStop phosphatase inhibitors (Roche)). 300 μg of the protein lysate was added with 3 μg of anti-Myc antibody 9E10 and allowed to rotate at 4°C for 1 hr, which was followed by addition of Protein A/G magnetic beads (Thermo Scientific) and rotation at 4°C for 1hr. Then the beads were collected and washed 3x with lysis buffer. Beads were then collected and treated with FastAP alkaline phosphatase (Thermo Scientific) for 30 min at 37°C and washed 3x with lysis buffer and 2x with kinase assay buffer (25 mM Tris pH 7.5, 5 mM beta glycerophosphate, 2 mM DTT and 0.1 mM sodium orthovanadate). CK1δ ΔC (200 ng) was incubated with either 1 mM of unphosphorylated mouse PER2 FASP peptide RKKK(642)TEVSAHLSSLTLPGKAESVVSLTSQ (Narasimamurthy *et al.*, 2018) or the

human PER2 4pFASP peptide GKAEpSVApSLTpSQCpSYA for 15 min at 25°C. The beads were split into three samples with kinase assay buffer containing 10 mM of magnesium chloride and 200 μM of ATP. The first portion was left untreated while the second and third were incubated with CK1δ-ΔC (200 ng) that had been pre-incubated with NP FASP or 4pFASP peptide, respectively, and incubated for 60 min at 25°C. The beads were collected, and protein was eluted by adding protein loading dye and analyzed by SDS-PAGE for Western blotting with anti-pSer659 antibody as previously described (Narasimamurthy *et al.*, 2018).

**Real-time PER2::LUC half-life measurement—**1 μg of the indicated human PER2::LUC expression plasmids (under a PGK promoter) were transiently transfected alone or with 100 ng myc-CK1ε (under a CMV promoter) in 35 mm dishes of HEK293T cells in MOPS-buffered high glucose media supplemented with D-luciferin (8.3g/L DMEM, 0.35 mg/mL sodium bicarbonate, 5 mg/mL glucose, 0.02 M MOPS, 100 U/mL penicillin, 100 μg/mL streptomycin, and 100 mM D-luciferin). Dishes were sealed with 40 mm cover glasses and vacuum grease (Sigma Aldrich), and then placed in a LumiCycle 32 (Actimetrics) at 37°C. 24 hrs post transfection, 40 μg/mL cycloheximide (Sigma) was added per 35 mm dish and luminescence recording was initiated. Luminescence data were used to calculate PER2::LUC half-life in Prism (GraphPad) using one-phase decay algorithm as described previously (Zhou *et al.*, 2015), beginning from the point of cycloheximide addition to the plateau at minimum luciferase activity ($n \geq 4$).

**Co-immunoprecipitation assays—**Human myc-PER2, FLAG-CK1δ and FLAG-β-TrCP expression plasmids (1.5 μg, 1.5 μg WT or 0.75 μg K38A, and 3 μg of plasmid DNA, respectively) were co-transfected in 60 mm dishes of HEK293T cells in DMEM supplemented with 1% penicllin/streptomycin and 10% HyClone FetalClone II FBS (Fisher Science). The proteasome was inhibited 16 hrs prior to harvest with 10 μM MG132 (Sigma Aldrich) and cells were harvested 72 hrs post transfection. Cells were lysed in 350 μL mammalian cell lysis buffer (20 mM Tris pH 7.5, 150 mM NaCl, 1mM TCEP, 1% NP-40) supplemented with EDTA-free protease inhibitors (Pierce) and phosphatase inhibitors (1 mM NaF, 1 mM β-glycerophosphate and 1 mM $Na_3VO_4$). 30 μL input samples were prepared with 2x SDS sample buffer, and the remaining lysate was incubated with 30 μL of anti-Myc agarose slurry (cat. #sc-40 AC, Santa Cruz Biotechnology) and tumbled overnight at 4°C. Bound samples were washed 3x with 400 μL of IP wash buffer (20 mM Tris pH 7.5, 150 mM NaCl) and 6x SDS sample buffer. All samples were briefly boiled at 95°C and resolved by 7.5% polyacrylamide-SDS gel electrophoresis (PAGE) and transferred to nitrocellulose membrane via Trans-Blot Turbo transfer system (Bio-Rad). Membranes were incubated in TBST blocking buffer (20 mM Tris pH 7.5, 150 mM NaCl, 0.1% TWEEN 20 and 5% (weight/vol, w/v) Marvel dried skimmed milk) for 1 hr and then incubated with antibody (1:2000 α-Myc HRP (cat. #sc-40 HRP), Santa Cruz Biotechnology) or 1/1000 α-OctA HRP (cat. #sc-166355 HRP, Santa Cruz Biotechnology)) in blocking buffer at 4°C overnight. Membranes were washed the next day 3x with TBST and chemiluminescence detection was performed using Immobilon reagent (Millipore) and imaged with ChemiDoc (Bio-Rad). Representative blot shown (n = 3).

**Crystallization and structure determination—**For crystallization experiments, a CK1 catalytic domain further truncated to include residues 1–294 was used instead of 1–317, given that no density was observed for residues 295–317 in previous crystal structures and to limit the possible disruption of peptide binding. All peptides were solubilized in a solution of 0.15 M Succinic Acid pH 5.5 and 20% (w/v) PEG 3350 and soaked overnight into crystals of human CK1δ (1–294) that were crystallized using the hanging drop vapor diffusion method as follows: the 4pFASP peptide was added to CK1δ crystals that were crystallized in 0.13 M Succinic Acid pH 5.5 and 27% (w/v) PEG 3350; the 3pFASP peptide was added to CK1δ crystals that were crystallized in 0.1 M Succinic Acid pH 5.5 and 15% (w/v) PEG 3350; the 2pFASP peptide was added to CK1δ crystals that were crystallized in 0.15 M Succinic Acid pH 5.5 and 22% (w/v) PEG 3350; and the pS589 peptide was added to CK1δ crystals that were crystallized in 0.16 M Succinic Acid pH 5.5 and 23% PEG (w/v) 3350. The crystals were looped and briefly soaked in a drop of cryo-preservation solution (80% peptide solution, 20% glycerol) and then flash-cooled in liquid nitrogen for X-ray diffraction data collection. Data sets were collected at the 23-ID-D beamline at the Advanced Photon Source (APS) at the Argonne National Laboratory. Data were indexed, integrated and merged using the CCP4 software suite (Winn et al., 2011). Structures were determined by molecular replacement with Phaser MR (McCoy et al., 2007) using the apo structure of wild-type CK1δ ΔC (PDB: 6PXO). Model building was performed with Coot (Emsley et al., 2010) and structure refinement was performed with PHENIX (Adams et al., 2011). All structural models and alignments were generated using PyMOL Molecular Graphics System 2.0 (Schrödinger). X-ray crystallography data collection and refinement statistics are provided in supplementary information (Table 1).

**pLogogram analysis—**The Comparative Site Search function of PhosphoSitePlus (v6.6.0.4) (Hornbeck, 2015) was used to obtain a list of known CK1δ substrates. The substrates were all limited to 15 residues in length with the center residue being the site of phosphorylation. The Sequence Logo Analysis tool from PhosphoSitePlus was used on the resulting dataset to generate a pLogogram indicating the relative frequency of amino acid types in positions flanking the site of phosphorylation.

## Molecular dynamics

**Molecular modeling:** To build the molecular model of 5pFASP-CK1, we started from the 3pFASP x-ray structure and then added E661 and residues 669 to 675 with Maestro (Schrodinger Release 2020-3) in a linear conformation. To avoid artificial interactions arising from the short size of the peptide, we capped the N- and C-terminal residues with acetyl (ACE) and N-methyl amine (NME) groups, respectively. Hydrogens were added with PrepWizard module, and a restrained minimization was to remove potential clashes between the modeled FASP peptide and the enzyme.

***System* preparation:** CK1-5pFASP complex was solvated in a pre-equilibrated TIP3P (Jorgensen et al., 1983) water box with at least 15 Å between the protein and the box boundaries. The net charge of the system was neutralized with a $Na^+$ ion. Parameters for protein residues, capping groups, and Na+ were obtained from ff14SB forcefield (Maier et al., 2015).

**Equilibration:** Minimization and equilibration were performed with AMBER16 (Case, 2016) using the following protocol: (i) 2000 steps of energy minimization with 500 kcal $mol^{-1}$ $Å^{-1}$ position restraints on all protein atoms; (ii) 5000 steps of energy minimization with 500 kcal $mol^{-1}$ $Å^{-1}$ position restraints on all CK1 atoms and on the backbone atoms of FASP; (iii) 5000 steps of energy minimization with 500 kcal $mol^{-1}$ $Å^{-1}$ position restraints on all backbone atoms; (iv) 5000 steps of energy minimization with 500 kcal $mol^{-1}$ $Å^{-1}$ position restraints on CK1 backbone atoms; (v) 5000 steps of energy minimization without any position restraints; (vi) 50 ps of NVT simulations, with gradual heating of the system to a final temperature of 300 K and 10 kcal $mol^{-1}$ $Å^{-1}$ position restraints on protein atoms; (vii) 1 ns of NPT simulation with 100 kcal $mol^{-1}$ $Å^{-1}$ position restraints on protein atoms; and (viii) 1 ns of NPT simulation to equilibrate the density (or final volume of the simulation box).

**Simulations:** Gaussian accelerated MD simulations (GaMD) were performed in the NVT regime, with a time step of 2 fs. The PME method was used to calculate electrostatic interactions with periodic boundary conditions (Darden et al., 1993). To accelerate sampling of the conformational space, we used boost parameters as described in (Miao *et al.*, 2015). All systems had a threshold energy $V = V_{max}$ and were subjected to a dual boost acceleration of both dihedral and total potential energies. To optimize the acceleration parameters, we first ran 2 ns of conventional MD simulation (without boost potentials) during which $V_{min}$, $V_{max}$, $V_{avg}$, and $\sigma_{avg}$ were recorded and used to calculate boost potentials as previously detailed (Miao *et al.*, 2015). These potentials were employed to start 50 ns of preparatory GaMD simulations, during which the boost statistics and boost potentials were updated until the maximum acceleration was achieved. The maximum acceleration was constrained by setting the upper limit of the standard deviation of the total boost potential to be ≤ 6 kcal/mol. Starting from the same equilibrated structure, we launched 10 independent GaMD simulations with different initial velocities. Each simulation ran for 100 ns, totalizing 1 μs of sampling time.

***In Cis* phosphorylation assay (mobility shift analysis)—**1:1 complexes of HGST-CK1δ (1–317):HNS-Degron-CK1BD-B TEV 507 were phosphorylated in 80 uL reactions (10 uM complex, 1 mM ATP, 10 mM $MgCl_2$, in FPLC buffer), and 5 uL aliquots were quenched at discrete timepoints using 5 uL of 2x EDTA (40 mM). 5 uL of 3x TEV protease (2 mg/mL) was added and TEV cleavage was performed at RT for 1hr. All samples were briefly boiled at 95°C and resolved by polyacrylamide-SDS gel electrophoresis (PAGE). The mobility shift of phosphorylated bands were analyzed using ImageJ (version 1.53), with the relative pixel density of each band was normalized to the corresponding band at 0 mins of the reaction.

**Bioluminescence recording of *Per*$^{Luc}$ reporter cell lines—**Cells were plated into 24-well plates or 35 mm dishes to be approximately 90% confluent 24 hours prior to the start of the experiment. Immediately before the start of the experiment, cells were given a two-hour serum shock with 50% horse serum in DMEM or 10 μM forskolin (Sigma Aldrich) in DMEM (Fig S5), washed with phosphate-buffered saline (PBS) and fresh DMEM supplemented with 1% FBS, 7.5 mM sodium bicarbonate, 10 mM HEPES, 25

U/mL penicillin, 25 μg/mL streptomycin, and 0.1 mM luciferin. The plates were sealed with cellophane tape and the dishes with a 40 mm cover glass and vacuum grease before placing them into a Lumicycle 32 or 96 (Actimetrics). For all bioluminescence experiments, the results were reproduced in at least two independent experiments. Real-time levels, period, and phase of the bioluminescence rhythms were evaluated using the Lumicycle software (Actimetrics). Student's t-test was used to compare data from WT and mutant cells.

**Circadian sampling and drug treatments in *Per*$^{Luc}$ reporter cell lines—**To measure PER rhythms in WT and mutant cells, cells were seeded in 60 mm dishes to be 90% confluent 24 hours prior to the experiment. These cells were treated with 50% horse serum in DMEM for 2 hrs and harvested at the indicated times. For cycloheximide (CHX) treatment, 8 μg/mL CHX (Sigma Aldrich) was added to cells and cells were collected at specified times after the treatment. For CHX washout experiments, cells were treated with CHX for 8 hrs followed by the normal DMEM, and cells were harvested at the indicated times after the CHX treatment.

**Immunoblotting of *Per*$^{Luc}$ reporter cell lines—**Cells were harvested from 60 mm dishes and flash-frozen on dry ice. Protein extraction and immunoblotting were performed as previously described (D'Alessandro *et al.*, 2015). Briefly, cells were homogenized at 4°C in 70 μL extraction buffer (EB) (0.4 M NaCl, 20 mM HEPES pH 7.5, 1 mM EDTA, 5 mM NaF, 1 mM dithiothreitol, 0.3% Triton X-100, 5% glycerol, 0.25 mM phenylmethylsulfonyl fluoride (PMSF), 10 mg/mL aprotinin, 5 mg/mL leupeptin, 1 mg/mL pepstatin A). Homogenates were cleared by centrifugation for 12 min at 12,000 g at 4°C. Supernatants were mixed with 2x SDS sample buffer and boiled. Proteins were separated by electrophoresis through SDS polyacrylamide gels and then transferred to nitrocellulose membranes. Membranes were blocked with 5% (w/v) non-fat dry milk in TBS-0.05% Tween-20 (TBST), incubated with primary antibodies (GP62 for PER1 and GP49 for PER2 (Jin *et al.*, 2019)) overnight followed by incubation with secondary antibodies for 1 h. The blots were developed using the WestFemto enhanced chemiluminescence substrate (Thermo Fisher Scientific).

***Drosophila* S2 cell experiments—**The plasmids pMT-*dbt*-V5, pAc-3XFLAG-His-d*per*/Tev100-6Xc-myc (Chiu *et al.*, 2008), pAc-d*per* WT (aa1-1224)-V5, pAc-d*per* S596A (aa1-1224)-V5 (Chiu *et al.*, 2011), pAc-d*per* WT (aa560-1034)-V5 (Ko et al., 2010) were previously described. pAc-d*per* S596A (aa560-1034)-V5 was generated via PCR mutagenesis using pAc-d*per* WT (aa560-1034)-V5 as a template as described in (Chiu *et al.*, 2011) and the QuikChange II site-directed mutagenesis kit (Agilent). *Drosophila* S2 cells and *Schneider's Drosophila* medium were obtained from Life Technologies (Thermo Fisher Scientific). S2 cells were seeded at $1 \times 10^6$ cells/mL in a 6-well plate and transfected using Effectene (Qiagen). S2 cells were co-transfected with 0.2 μg of pMT-*dbt*-V5, 0.8 μg of pAc-3X-FLAG-His-d*per*/Tev100-6Xc-myc, and varying amounts of d*per*-V5 plasmids as indicated. Expression of *dbt* was induced with 500 μM $CuSO_4$ 36 hours after transfection. Cells were harvested at the indicated time points after kinase induction and extracted with 100–150 μL EB2 (20 mM Hepes pH 7.5, 100 mM KCl, 5% glycerol, 5 mM EDTA, 1 mM DTT, 0.1% Triton X-100, 25 mM NaF, 0.5 mM PMSF).

1 μL of AcTEV protease (Thermo Fisher Scientific) was added to protein extracts and incubated 16 hours at 4°C. Following TEV cleavage, protein concentration was measured using Pierce Coomassie Plus Assay Reagents (Thermo Fisher Scientific). 2X SDS sample buffer was added, and the mixture boiled at 95°C for 5 minutes. Equal amounts of proteins were resolved by 16% polyacrylamide-SDS gel electrophoresis (PAGE) and transferred to nitrocellulose membrane (Bio-Rad) using a Semi-Dry Transfer Cell (Bio-Rad). Membranes were incubated in 5% Blocking Buffer (Bio-Rad) for 40 minutes at room temperature, and then incubated with anti-FLAG (cat. # F1804, Millipore Sigma) at 1:7000 for 16–20 hours at room temperature. Blots were washed with 1X TBST for 1 hour, incubated with anti-mouse IgG HRP (cat. #12-349, Millipore Sigma) at 1:2000 for 1 hour. After washing, chemiluminescence detection was performed using Clarity ECL reagent in combination with the ChemiDoc imager (Bio-Rad). ImageJ Version 2.0.0-rc-67/1.52d (NIH) was used to quantify hypo-phosphorylated PER and nonspecific signals (indicated by asterisks). PER signal was normalized to nonspecific signal and the data were scaled with normalized PER signal at 0 hr to a value of 1. Two-way ANOVA with Sidak multiple comparisons test was performed using Prism (GraphPad).

### QUANTIFICATION AND STATISTICAL ANALYSIS

All statistical analyses were done using Prism (Graphpad). P-values were calculated using Students t-test, one-way ANOVA with Tukey's multiple comparisons test, or two-way ANOVA with Sidak multiple comparisons test as indicated in different figures. In all figures, * indicates $p<0.05$, **$p<0.01$, ***$p<0.001$, ****$p<0.0001$; ns, not significant.

## Supplementary Material

Refer to Web version on PubMed Central for supplementary material.

## Acknowledgements

We thank the staff at the 23-ID-D beamline at the Advanced Photon Source of the Argonne National Lab for their help with data collection. Funding for this work was provided by the US National Institutes of Health grants R01 GM107069 and R35 GM141849 (to C.L.P.), and Singapore Ministry of Health grant MOH-000600 to D.M.V. S.R.H. was supported by an NIH fellowship F32 GM133149.

## References

Adams PD, Afonine PV, Bunkoczi G, Chen VB, Echols N, Headd JJ, Hung LW, Jain S, Kapral GJ, Grosse Kunstleve RW, et al. (2011). The Phenix software for automated determination of macromolecular structures. Methods 55, 94–106. 10.1016/j.ymeth.2011.07.005. [PubMed: 21821126]

An Y, Yuan B, Xie P, Gu Y, Liu Z, Wang T, Li Z, Xu Y, and Liu Y (2022). Decoupling PER phosphorylation, stability and rhythmic expression from circadian clock function by abolishing PER-CK1 interaction. Nat Commun 13, 3991. 10.1038/s41467-022-31715-4. [PubMed: 35810166]

Aryal RP, Kwak PB, Tamayo AG, Gebert M, Chiu PL, Walz T, and Weitz CJ (2017). Macromolecular Assemblies of the Mammalian Circadian Clock. Mol Cell 67, 770–782 e776. 10.1016/j.molcel.2017.07.017. [PubMed: 28886335]

Baylies MK, Vosshall LB, Sehgal A, and Young MW (1992). New short period mutations of the Drosophila clock gene per. Neuron 9, 575–581. 10.1016/0896-6273(92)90194-i. [PubMed: 1524831]

Beesley S, Kim DW, D'Alessandro M, Jin Y, Lee K, Joo H, Young Y, Tomko RJ Jr., Faulkner J, Gamsby J, et al. (2020). Wake-sleep cycles are severely disrupted by diseases affecting cytoplasmic homeostasis. Proc Natl Acad Sci U S A 117, 28402–28411. 10.1073/pnas.2003524117. [PubMed: 33106420]

Cao X, Yang Y, Selby CP, Liu Z, and Sancar A (2021). Molecular mechanism of the repressive phase of the mammalian circadian clock. Proc Natl Acad Sci U S A 118. 10.1073/pnas.2021174118.

Case DA, Betz RM, Cerutti DS, Cheatham DE III, Darden TA, Duke RE, Giese TJ, Gohlke H, Goetz AW, Homeyer N, et al. (2016). AMBER 16.

Cegielska A, Gietzen KF, Rivers A, and Virshup DM (1998). Autoinhibition of casein kinase I epsilon (CKI epsilon) is relieved by protein phosphatases and limited proteolysis. J Biol Chem 273, 1357–1364. 10.1074/jbc.273.3.1357. [PubMed: 9430669]

Chen R, Schirmer A, Lee Y, Lee H, Kumar V, Yoo SH, Takahashi JS, and Lee C (2009). Rhythmic PER abundance defines a critical nodal point for negative feedback within the circadian clock mechanism. Mol Cell 36, 417–430. 10.1016/j.molcel.2009.10.012. [PubMed: 19917250]

Chiou YY, Yang Y, Rashid N, Ye R, Selby CP, and Sancar A (2016). Mammalian Period represses and de-represses transcription by displacing CLOCK-BMAL1 from promoters in a Cryptochrome-dependent manner. Proc Natl Acad Sci U S A 113, E6072–E6079. 10.1073/pnas.1612917113. [PubMed: 27688755]

Chiu JC, Ko HW, and Edery I (2011). NEMO/NLK phosphorylates PERIOD to initiate a time-delay phosphorylation circuit that sets circadian clock speed. Cell 145, 357–370. 10.1016/j.cell.2011.04.002. [PubMed: 21514639]

Chiu JC, Vanselow JT, Kramer A, and Edery I (2008). The phospho-occupancy of an atypical SLIMB-binding site on PERIOD that is phosphorylated by DOUBLETIME controls the pace of the clock. Genes Dev 22, 1758–1772. 10.1101/gad.1682708. [PubMed: 18593878]

Cordier F, Chaffotte A, Terrien E, Prehaud C, Theillet FX, Delepierre M, Lafon M, Buc H, and Wolff N (2012). Ordered phosphorylation events in two independent cascades of the PTEN C-tail revealed by NMR. J Am Chem Soc 134, 20533–20543. 10.1021/ja310214g. [PubMed: 23171049]

Crosby P, and Partch CL (2020). New insights into non-transcriptional regulation of mammalian core clock proteins. J Cell Sci 133. 10.1242/jcs.241174.

Cullati SN, Chaikuad A, Chen JS, Gebel J, Tesmer L, Zhubi R, Navarrete-Perea J, Guillen RX, Gygi SP, Hummer G, et al. (2022). Kinase domain autophosphorylation rewires the activity and substrate specificity of CK1 enzymes. Mol Cell. 10.1016/j.molcel.2022.03.005.

D'Alessandro M, Beesley S, Kim JK, Chen R, Abich E, Cheng W, Yi P, Takahashi JS, and Lee C (2015). A tunable artificial circadian clock in clock-defective mice. Nat Commun 6, 8587. 10.1038/ncomms9587. [PubMed: 26617050]

Darden T, York D, and Pedersen L (1993). Particle Mesh Ewald - an N.Log(N) Method for Ewald Sums in Large Systems. J Chem Phys 98, 10089–10092. Doi 10.1063/1.464397.

Delaglio F, Grzesiek S, Vuister GW, Zhu G, Pfeifer J, and Bax A (1995). NMRPipe: a multidimensional spectral processing system based on UNIX pipes. Journal of biomolecular NMR 6, 277–293. [PubMed: 8520220]

Durgan DJ, Pat BM, Laczy B, Bradley JA, Tsai JY, Grenett MH, Ratcliffe WF, Brewer RA, Nagendran J, Villegas-Montoya C, et al. (2011). O-GlcNAcylation, novel post-translational modification linking myocardial metabolism and cardiomyocyte circadian clock. J Biol Chem 286, 44606–44619. 10.1074/jbc.M111.278903. [PubMed: 22069332]

Dyla M, Gonzalez Foutel NS, Otzen DE, and Kjaergaard M (2022). The optimal docking strength for reversibly tethered kinases. Proc Natl Acad Sci U S A 119, e2203098119. 10.1073/pnas.2203098119. [PubMed: 35696590]

Eide EJ, Woolf MF, Kang H, Woolf P, Hurst W, Camacho F, Vielhaber EL, Giovanni A, and Virshup DM (2005). Control of mammalian circadian rhythm by CKIepsilon-regulated proteasome-mediated PER2 degradation. Mol Cell Biol 25, 2795–2807. 10.1128/MCB.25.7.2795-2807.2005. [PubMed: 15767683]

Emsley P, Lohkamp B, Scott WG, and Cowtan K (2010). Features and development of Coot. Acta Crystallogr D Biol Crystallogr 66, 486–501. 10.1107/S0907444910007493. [PubMed: 20383002]

Flotow H, Graves PR, Wang AQ, Fiol CJ, Roeske RW, and Roach PJ (1990). Phosphate groups as substrate determinants for casein kinase I action. J Biol Chem 265, 14264–14269. [PubMed: 2117608]

Flotow H, and Roach PJ (1991). Role of acidic residues as substrate determinants for casein kinase I. J Biol Chem 266, 3724–3727. [PubMed: 1995625]

Fustin JM, Kojima R, Itoh K, Chang HY, Ye S, Zhuang B, Oji A, Gibo S, Narasimamurthy R, Virshup D, et al. (2018). Two Ck1delta transcripts regulated by m6A methylation code for two antagonistic kinases in the control of the circadian clock. Proc Natl Acad Sci U S A 115, 5980–5985. 10.1073/pnas.1721371115. [PubMed: 29784786]

Gallego M, Eide EJ, Woolf MF, Virshup DM, and Forger DB (2006a). An opposite role for tau in circadian rhythms revealed by mathematical modeling. Proc Natl Acad Sci U S A 103, 10618–10623. 10.1073/pnas.0604511103. [PubMed: 16818876]

Gallego M, Kang H, and Virshup DM (2006b). Protein phosphatase 1 regulates the stability of the circadian protein PER2. Biochem J 399, 169–175. 10.1042/Bj20060678. [PubMed: 16813562]

Gebel J, Tuppi M, Chaikuad A, Hotte K, Schroder M, Schulz L, Lohr F, Gutfreund N, Finke F, Henrich E, et al. (2020). p63 uses a switch-like mechanism to set the threshold for induction of apoptosis. Nat Chem Biol 16, 1078–1086. 10.1038/s41589-020-0600-3. [PubMed: 32719556]

Graves PR, and Roach PJ (1995). Role of COOH-terminal phosphorylation in the regulation of casein kinase I delta. J Biol Chem 270, 21689–21694. 10.1074/jbc.270.37.21689. [PubMed: 7665585]

He Q, Cha J, He Q, Lee HC, Yang Y, and Liu Y (2006). CKI and CKII mediate the FREQUENCY-dependent phosphorylation of the WHITE COLLAR complex to close the Neurospora circadian negative feedback loop. Genes Dev 20, 2552–2565. 10.1101/gad.1463506. [PubMed: 16980584]

Hornbeck PV, Zhang B, Murray B, Kornhauser JM, Latham V, Skrzypek E (2015). PhosphSitePlus, 2014: mutations, PTMs and recalibrations. Nucleic Acids Res. 43:D512–20. [PubMed: 25514926]

Isojima Y, Nakajima M, Ukai H, Fujishima H, Yamada RG, Masumoto KH, Kiuchi R, Ishida M, Ukai-Tadenuma M, Minami Y, et al. (2009). CKIepsilon/delta-dependent phosphorylation is a temperature-insensitive, period-determining process in the mammalian circadian clock. Proc Natl Acad Sci U S A 106, 15744–15749. 10.1073/pnas.0908733106. [PubMed: 19805222]

Jeon M, Gardner HF, Miller EA, Deshler J, and Rougvie AE (1999). Similarity of the C. elegans developmental timing protein LIN-42 to circadian rhythm proteins. Science 286, 1141–1146. 10.1126/science.286.5442.1141. [PubMed: 10550049]

Jin YH, Joo H, Lee K, Kim H, Didier R, Yang Y, Shin H, and Lee C (2019). Streamlined procedure for gene knockouts using all-in-one adenoviral CRISPR-Cas9. Sci Rep 9, 277. 10.1038/s41598-018-36736-y. [PubMed: 30670765]

Jones CR, Huang AL, Ptacek LJ, and Fu YH (2013). Genetic basis of human circadian rhythm disorders. Exp Neurol 243, 28–33. 10.1016/j.expneurol.2012.07.012. [PubMed: 22849821]

Jorgensen WL, Chandrasekhar J, Madura JD, Impey RW, and Klein ML (1983). Comparison of Simple Potential Functions for Simulating Liquid Water. J Chem Phys 79, 926–935. Doi 10.1063/1.445869.

Kaasik K, Kivimae S, Allen JJ, Chalkley RJ, Huang Y, Baer K, Kissel H, Burlingame AL, Shokat KM, Ptacek LJ, and Fu YH (2013). Glucose sensor O-GlcNAcylation coordinates with phosphorylation to regulate circadian clock. Cell Metab 17, 291–302. 10.1016/j.cmet.2012.12.017. [PubMed: 23395175]

Kim EY, Ko HW, Yu WJ, Hardin PE, and Edery I (2007). A DOUBLETIME kinase binding domain on the Drosophila PERIOD protein is essential for its hyperphosphorylation, transcriptional repression, and circadian clock function. Molecular and Cellular Biology 27, 5014–5028. 10.1128/Mcb.02339-06. [PubMed: 17452449]

Kivimae S, Saez L, and Young MW (2008). Activating PER repressor through a DBT-directed phosphorylation switch. PLoS Biol 6, e183. 10.1371/journal.pbio.0060183. [PubMed: 18666831]

Ko HW, Kim EY, Chiu J, Vanselow JT, Kramer A, and Edery I (2010). A hierarchical phosphorylation cascade that regulates the timing of PERIOD nuclear entry reveals novel roles for proline-directed kinases and GSK-3beta/SGG in circadian clocks. J Neurosci 30, 12664–12675. 10.1523/JNEUROSCI.1586-10.2010. [PubMed: 20861372]

Koike N, Yoo SH, Huang HC, Kumar V, Lee C, Kim TK, and Takahashi JS (2012). Transcriptional architecture and chromatin landscape of the core circadian clock in mammals. Science 338, 349–354. 10.1126/science.1226339. [PubMed: 22936566]

Konopka RJ, and Benzer S (1971). Clock mutants of Drosophila melanogaster. Proc Natl Acad Sci U S A 68, 2112–2116. 10.1073/pnas.68.9.2112. [PubMed: 5002428]

Lee C, Etchegaray JP, Cagampang FR, Loudon AS, and Reppert SM (2001). Posttranslational mechanisms regulate the mammalian circadian clock. Cell 107, 855–867. 10.1016/s0092-8674(01)00610-9. [PubMed: 11779462]

Lee C, Weaver DR, and Reppert SM (2004). Direct association between mouse PERIOD and CKIepsilon is critical for a functioning circadian clock. Mol Cell Biol 24, 584–594. 10.1128/MCB.24.2.584-594.2004. [PubMed: 14701732]

Lee HM, Chen RM, Kim H, Etchegaray JP, Weaver DR, and Lee C (2011a). The period of the circadian oscillator is primarily determined by the balance between casein kinase 1 and protein phosphatase 1. P Natl Acad Sci USA 108, 16451–16456. 10.1073/pnas.1107178108.

Lee Y, Chen R, Lee HM, and Lee C (2011b). Stoichiometric relationship among clock proteins determines robustness of circadian rhythms. J Biol Chem 286, 7033–7042. 10.1074/jbc.M110.207217. [PubMed: 21199878]

Levine DC, Hong H, Weidemann BJ, Ramsey KM, Affinati AH, Schmidt MS, Cedernaes J, Omura C, Braun R, Lee C, et al. (2020). NAD(+) Controls Circadian Reprogramming through PER2 Nuclear Translocation to Counter Aging. Mol Cell 78, 835–849 e837. 10.1016/j.molcel.2020.04.010. [PubMed: 32369735]

Liu X, Chen A, Caicedo-Casso A, Cui G, Du M, He Q, Lim S, Kim HJ, Hong CI, and Liu Y (2019). FRQ-CK1 interaction determines the period of circadian rhythms in Neurospora. Nat Commun 10, 4352. 10.1038/s41467-019-12239-w. [PubMed: 31554810]

Longenecker KL, Roach PJ, and Hurley TD (1996). Three-dimensional structure of mammalian casein kinase I: molecular basis for phosphate recognition. J Mol Biol 257, 618–631. 10.1006/jmbi.1996.0189. [PubMed: 8648628]

Lowrey PL, Shimomura K, Antoch MP, Yamazaki S, Zemenides PD, Ralph MR, Menaker M, and Takahashi JS (2000). Positional syntenic cloning and functional characterization of the mammalian circadian mutation tau. Science 288, 483–492. 10.1126/science.288.5465.483. [PubMed: 10775102]

Maier JA, Martinez C, Kasavajhala K, Wickstrom L, Hauser KE, and Simmerling C (2015). ff14SB: Improving the Accuracy of Protein Side Chain and Backbone Parameters from ff99SB. Journal of Chemical Theory and Computation 11, 3696–3713. 10.1021/acs.jctc.5b00255. [PubMed: 26574453]

Marin O, Bustos VH, Cesaro L, Meggio F, Pagano MA, Antonelli M, Allende CC, Pinna LA, and Allende JE (2003). A noncanonical sequence phosphorylated by casein kinase 1 in beta-catenin may play a role in casein kinase 1 targeting of important signaling proteins. Proc Natl Acad Sci U S A 100, 10193–10200. 10.1073/pnas.1733909100. [PubMed: 12925738]

Marzoll D, Serrano FE, Shostak A, Schunke C, Diernfellner ACR, and Brunner M (2022). Casein kinase 1 and disordered clock proteins form functionally equivalent, phospho-based circadian modules in fungi and mammals. Proc Natl Acad Sci U S A 119. 10.1073/pnas.2118286119.

Masuda S, Narasimamurthy R, Yoshitane H, Kim JK, Fukada Y, and Virshup DM (2020). Mutation of a PER2 phosphodegron perturbs the circadian phosphoswitch. Proc Natl Acad Sci U S A 117, 10888–10896. 10.1073/pnas.2000266117. [PubMed: 32354999]

McCoy AJ, Grosse-Kunstleve RW, Adams PD, Winn MD, Storoni LC, and Read RJ (2007). Phaser crystallographic software. J Appl Crystallogr 40, 658–674. 10.1107/S0021889807021206. [PubMed: 19461840]

Miao Y, Feher VA, and McCammon JA (2015). Gaussian Accelerated Molecular Dynamics: Unconstrained Enhanced Sampling and Free Energy Calculation. J Chem Theory Comput 11, 3584–3595. 10.1021/acs.jctc.5b00436. [PubMed: 26300708]

Michael AK, Fribourgh JL, Chelliah Y, Sandate CR, Hura GL, Schneidman-Duhovny D, Tripathi SM, Takahashi JS, and Partch CL (2017). Formation of a repressive complex in the mammalian

circadian clock is mediated by the secondary pocket of CRY1. Proc Natl Acad Sci U S A 114, 1560–1565. 10.1073/pnas.1615310114. [PubMed: 28143926]

Narasimamurthy R, Hunt SR, Lu Y, Fustin JM, Okamura H, Partch CL, Forger DB, Kim JK, and Virshup DM (2018). CK1delta/epsilon protein kinase primes the PER2 circadian phosphoswitch. Proc Natl Acad Sci U S A 115, 5986–5991. 10.1073/pnas.1721076115. [PubMed: 29784789]

Nawathean P, Stoleru D, and Rosbash M (2007). A small conserved domain of Drosophila PERIOD is important for circadian phosphorylation, nuclear localization, and transcriptional repressor activity. Mol Cell Biol 27, 5002–5013. 10.1128/MCB.02338-06. [PubMed: 17452453]

Nolen B, Taylor S, and Ghosh G (2004). Regulation of protein kinases; controlling activity through activation segment conformation. Mol Cell 15, 661–675. 10.1016/j.molcel.2004.08.024. [PubMed: 15350212]

Ohsaki K, Oishi K, Kozono Y, Nakayama K, Nakayama KI, and Ishida N (2008). The role of {beta}-TrCP1 and {beta}-TrCP2 in circadian rhythm generation by mediating degradation of clock protein PER2. J Biochem 144, 609–618. 10.1093/jb/mvn112. [PubMed: 18782782]

Park JL, K; Kim H; Shin H; Lee C (2022). Endogenous circadian reporter cell lines as an efficient platform for studying circadian mechanisms. Co-submitted with this manuscript.

Philpott JM, Narasimamurthy R, Ricci CG, Freeberg AM, Hunt SR, Yee LE, Pelofsky RS, Tripathi S, Virshup DM, and Partch CL (2020). Casein kinase 1 dynamics underlie substrate selectivity and the PER2 circadian phosphoswitch. Elife 9. 10.7554/eLife.52343.

Reischl S, Vanselow K, Westermark PO, Thierfelder N, Maier B, Herzel H, and Kramer A (2007). Beta-TrCP1-mediated degradation of PERIOD2 is essential for circadian dynamics. J Biol Rhythms 22, 375–386. 10.1177/0748730407303926. [PubMed: 17876059]

Rivers A, Gietzen KF, Vielhaber E, and Virshup DM (1998). Regulation of casein kinase I epsilon and casein kinase I delta by an in vivo futile phosphorylation cycle. J Biol Chem 273, 15980–15984. 10.1074/jbc.273.26.15980. [PubMed: 9632646]

Rothenfluh A, Abodeely M, and Young MW (2000). Short-period mutations of per affect a double-time-dependent step in the Drosophila circadian clock. Curr Biol 10, 1399–1402. 10.1016/s0960-9822(00)00786-7. [PubMed: 11084344]

Rutila JE, Edery I, Hall JC, and Rosbash M (1992). The analysis of new short-period circadian rhythm mutants suggests features of D. melanogaster period gene function. J Neurogenet 8, 101–113. 10.3109/01677069209084155. [PubMed: 1634995]

Sathyanarayanan S, Zheng X, Xiao R, and Sehgal A (2004). Posttranslational regulation of Drosophila PERIOD protein by protein phosphatase 2A. Cell 116, 603–615. 10.1016/s0092-8674(04)00128-x. [PubMed: 14980226]

Schmutz I, Wendt S, Schnell A, Kramer A, Mansuy IM, and Albrecht U (2011). Protein Phosphatase 1 (PP1) Is a Post-Translational Regulator of the Mammalian Circadian Clock. Plos One 6. ARTN e21325 10.1371/journal.pone.0021325.

Sheffield P, Garrard S, and Derewenda Z (1999). Overcoming expression and purification problems of RhoGDI using a family of “parallel” expression vectors. Protein Expr Purif 15, 34–39. 10.1006/prep.1998.1003. [PubMed: 10024467]

Shinohara Y, Koyama YM, Ukai-Tadenuma M, Hirokawa T, Kikuchi M, Yamada RG, Ukai H, Fujishima H, Umehara T, Tainaka K, and Ueda HR (2017). Temperature-Sensitive Substrate and Product Binding Underlie Temperature-Compensated Phosphorylation in the Clock. Mol Cell 67, 783–798 e720. 10.1016/j.molcel.2017.08.009. [PubMed: 28886336]

Smith MJ, Marshall CB, Theillet FX, Binolfi A, Selenko P, and Ikura M (2015). Real-time NMR monitoring of biological activities in complex physiological environments. Curr Opin Struct Biol 32, 39–47. 10.1016/j.sbi.2015.02.003. [PubMed: 25727665]

Takahashi JS (2017). Transcriptional architecture of the mammalian circadian clock. Nat Rev Genet 18, 164–179. 10.1038/nrg.2016.150. [PubMed: 27990019]

Toh KL, Jones CR, He Y, Eide EJ, Hinz WA, Virshup DM, Ptacek LJ, and Fu YH (2001). An hPer2 phosphorylation site mutation in familial advanced sleep phase syndrome. Science 291, 1040–1043. 10.1126/science.1057499. [PubMed: 11232563]

Top D, O’Neil JL, Merz GE, Dusad K, Crane BR, and Young MW (2018). CK1/Doubletime activity delays transcription activation in the circadian clock. Elife 7. 10.7554/eLife.32679.

Vanselow K, Vanselow JT, Westermark PO, Reischl S, Maier B, Korte T, Herrmann A, Herzel H, Schlosser A, and Kramer A (2006). Differential effects of PER2 phosphorylation: molecular basis for the human familial advanced sleep phase syndrome (FASPS). Genes Dev 20, 2660–2672. 10.1101/gad.397006. [PubMed: 16983144]

Venkatesan A, Fan JY, Bouyain S, and Price JL (2019). The Circadian tau Mutation in Casein Kinase 1 Is Part of a Larger Domain That Can Be Mutated to Shorten Circadian Period. Int J Mol Sci 20. 10.3390/ijms20040813.

Vranken WF, Boucher W, Stevens TJ, Fogh RH, Pajon A, Llinas M, Ulrich EL, Markley JL, Ionides J, and Laue ED (2005). The CCPN data model for NMR spectroscopy: development of a software pipeline. Proteins 59, 687–696. 10.1002/prot.20449. [PubMed: 15815974]

Winn MD, Ballard CC, Cowtan KD, Dodson EJ, Emsley P, Evans PR, Keegan RM, Krissinel EB, Leslie AG, McCoy A, et al. (2011). Overview of the CCP4 suite and current developments. Acta Crystallogr D Biol Crystallogr 67, 235–242. 10.1107/S0907444910045749. [PubMed: 21460441]

Wu G, Xu G, Schulman BA, Jeffrey PD, Harper JW, and Pavletich NP (2003). Structure of a beta-TrCP1-Skp1-beta-catenin complex: destruction motif binding and lysine specificity of the SCF(beta-TrCP1) ubiquitin ligase. Mol Cell 11, 1445–1456. 10.1016/s1097-2765(03)00234-x. [PubMed: 12820959]

Xu Y, Padiath QS, Shapiro RE, Jones CR, Wu SC, Saigoh N, Saigoh K, Ptacek LJ, and Fu YH (2005). Functional consequences of a CKIdelta mutation causing familial advanced sleep phase syndrome. Nature 434, 640–644. 10.1038/nature03453. [PubMed: 15800623]

Xu Y, Toh KL, Jones CR, Shin JY, Fu YH, and Ptacek LJ (2007). Modeling of a human circadian mutation yields insights into clock regulation by PER2. Cell 128, 59–70. 10.1016/j.cell.2006.11.043. [PubMed: 17218255]

Yu W, Zheng H, Price JL, and Hardin PE (2009). DOUBLETIME plays a noncatalytic role to mediate CLOCK phosphorylation and repress CLOCK-dependent transcription within the Drosophila circadian clock. Mol Cell Biol 29, 1452–1458. 10.1128/MCB.01777-08. [PubMed: 19139270]

Zeringo NA, and Bellizzi JJ 3rd (2014). A PER2-derived mechanism-based bisubstrate analog for casein kinase 1epsilon. Chem Biol Drug Des 84, 697–703. 10.1111/cbdd.12363. [PubMed: 24985607]

Zhou M, Kim JK, Eng GW, Forger DB, and Virshup DM (2015). A Period2 Phosphoswitch Regulates and Temperature Compensates Circadian Period. Mol Cell 60, 77–88. 10.1016/j.molcel.2015.08.022. [PubMed: 26431025]

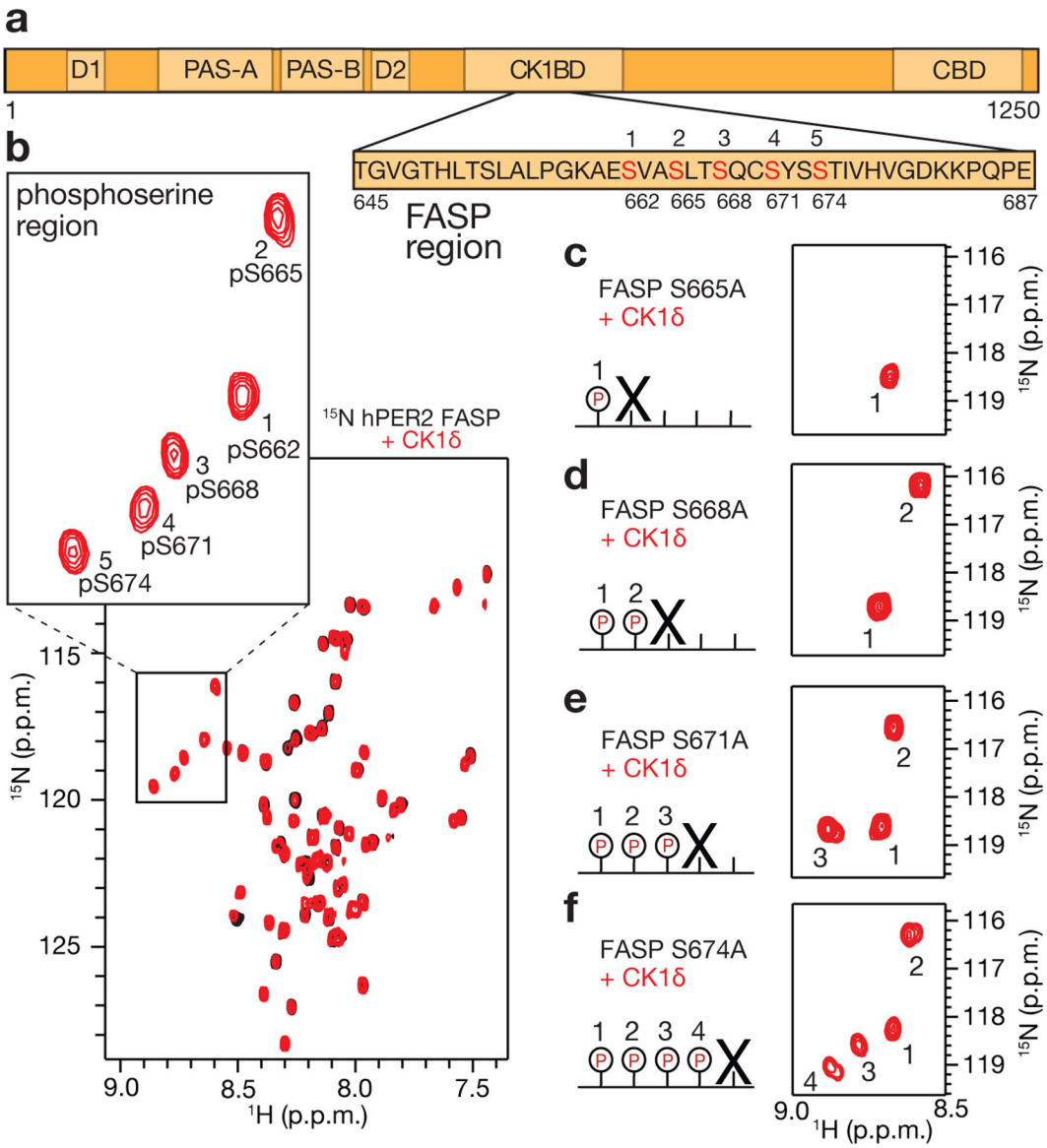


**Figure 1. CK1 phosphorylates the human PER2 FASP region sequentially.**

**a**, Domain map of hPER2 with tandem PAS domains, phosphodegrons (D1/D2), Casein Kinase 1 binding domain (CK1BD), and CRY binding domain (CBD). Zoom, the FASP peptide used in NMR assays with CK1 phosphorylation sites (red). **b**, $^{15}N/^{1}H$ HSQC of 200 μM hPER2 FASP used for kinetic assays (black), overlayed with 16 hr timepoint in kinase assay (red). Zoom/boxed region, the phosphoserine region. Numbering (1–5) corresponds to the order in the FASP peptide. **c-f**, Schematic representation of Ser/Ala mutations introduced to the FASP peptide. X, indicates position of the alanine substitution within the FASP serine cluster. Zoom of phosphoserine region for the $^{15}N/^{1}H$ HSQC of FASP mutants (red) at 3 hr timepoint in the kinase assay, with numbering showing the sequential order of reaction.

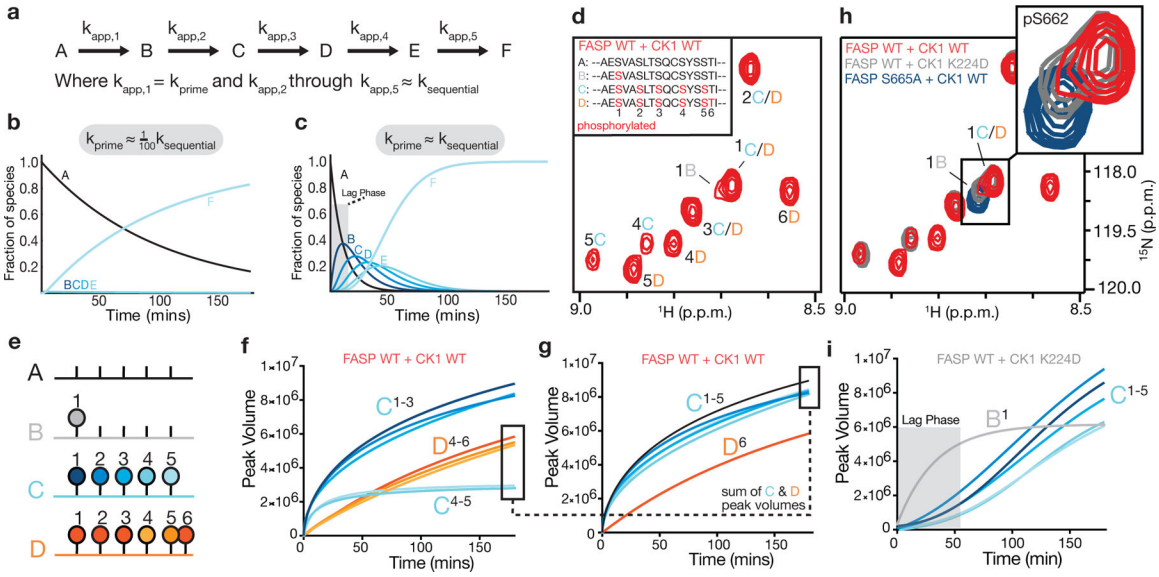


**Figure 2. CK1 follows an ordered distributive mechanism on the human PER2 FASP region.**

**a**, Schematic of ordered distributive kinetic model used for panels **b** and **c** (modeled using Wolfram Mathematica, see Supplement). **b**, Reaction coordinate for ordered distributive kinetic mechanism with differential rates for priming and sequential kinase activity. **c**, Reaction coordinate for ordered distributive kinetic mechanism with similar rates for priming and sequential kinase activity. **d**, Zoom of $^{15}N/^{1}H$ HSQC hPER2 FASP phosphoserine region looking at peaks corresponding to different states arising from at 3 hr incubation with CK1 WT (red). States A-D (inset) correspond to unique chemical shift states observed throughout the kinase assay. **e**, Schematic of unique states A-D observed in **d**: A, unphosphorylated FASP; B, primed FASP; C, all serines in FASP phosphorylated; D, all serines plus T675 phosphorylated. Numbering indicates order of phosphorylation. **f**, Traces of accumulating peak volume from the NMR kinase assay. Letters C-D with superscript numbers correspond to specific phosphoserines observed in the NMR assay. **g**, Same traces as in **f**, with peak volumes corresponding to states C and D for the last two serines (4–5) summed to show that all phosphoserines in the FASP report on state C with similar kinetics. **h**, Phosphoserine region showing unique chemical shift environment for singly phosphorylated (priming only) FASP S665A (blue) overlayed with WT FASP with CK1 WT (red) or K224D (gray) after 3 hr incubation. B-D lettering corresponds to unique states observed in NMR kinase assay as in **d**. **i**, Traces of accumulating peak volume from NMR kinase assay with CK1 K224D, resolving the transient accumulation of primed FASP and a clear lagging phase for subsequent phosphorylation states.

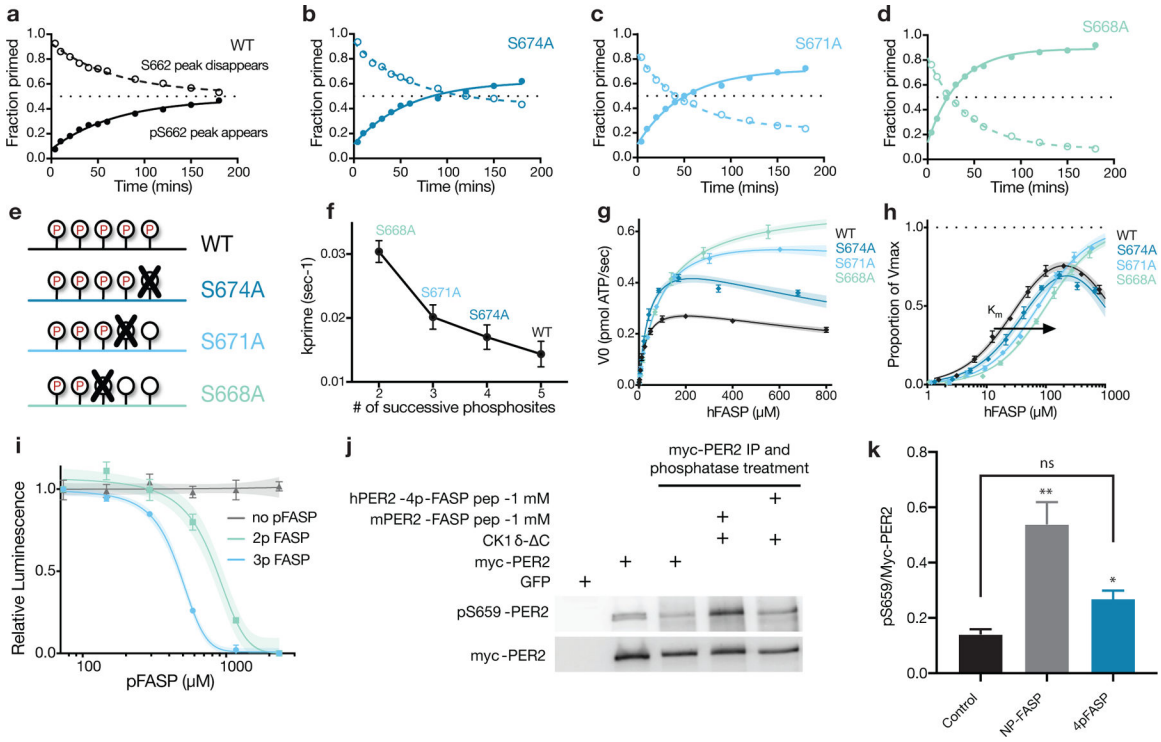


**Figure 3. Phosphorylation of the human PER2 FASP region inhibits CK1 activity.**

**a-d**, NMR kinase assay for the WT FASP or indicated mutant peptides monitoring the reaction kinetics of priming phosphorylation at S662 by NMR. **e**, Schematic of FASP alanine mutations and resulting discrete phosphostates. **f**, Plot of priming rate constant ($k_{prime}$) as a function of the possible successive phosphosites in the FASP. Error bars represent SEM from fits in panels **a-d**. **g**, ADP-Glo kinase assay with titration of FASP mutant peptides with mean and SD from 2 replicates, representative of n = 3 independent assays. Shaded area indicates 95% C.I. of the fit. **h**, Data from panel **f** normalized by $V_{max}$ values calculated from the preferred kinetic model (see Supplementary Figure 2, Table 1). **i**, ADP-Glo kinase assay of hPER2 PAS-degron peptide (see Supplementary Figure 2b) with titration of pFASP peptides corresponding to 2 (2p) or 3 (3p) phosphoserines (see Supplementary Figure 3a) with mean and SD from 2 replicates, representative of n = 3 independent assays. Shaded area indicates 95% C.I. of the fit. **j-k**, Western blot and quantification of the phosphorylation of the FASP priming site (pS659 in mouse PER2). Full-length mouse PER2 was immunoprecipitated from transfected HEK293T cells, dephosphorylated, and subjected to an *in vitro* kinase assay with 200 ng CK1 in the presence and absence of unphosphorylated mouse PER2 FASP or human PER2 4pFASP peptides as indicated.

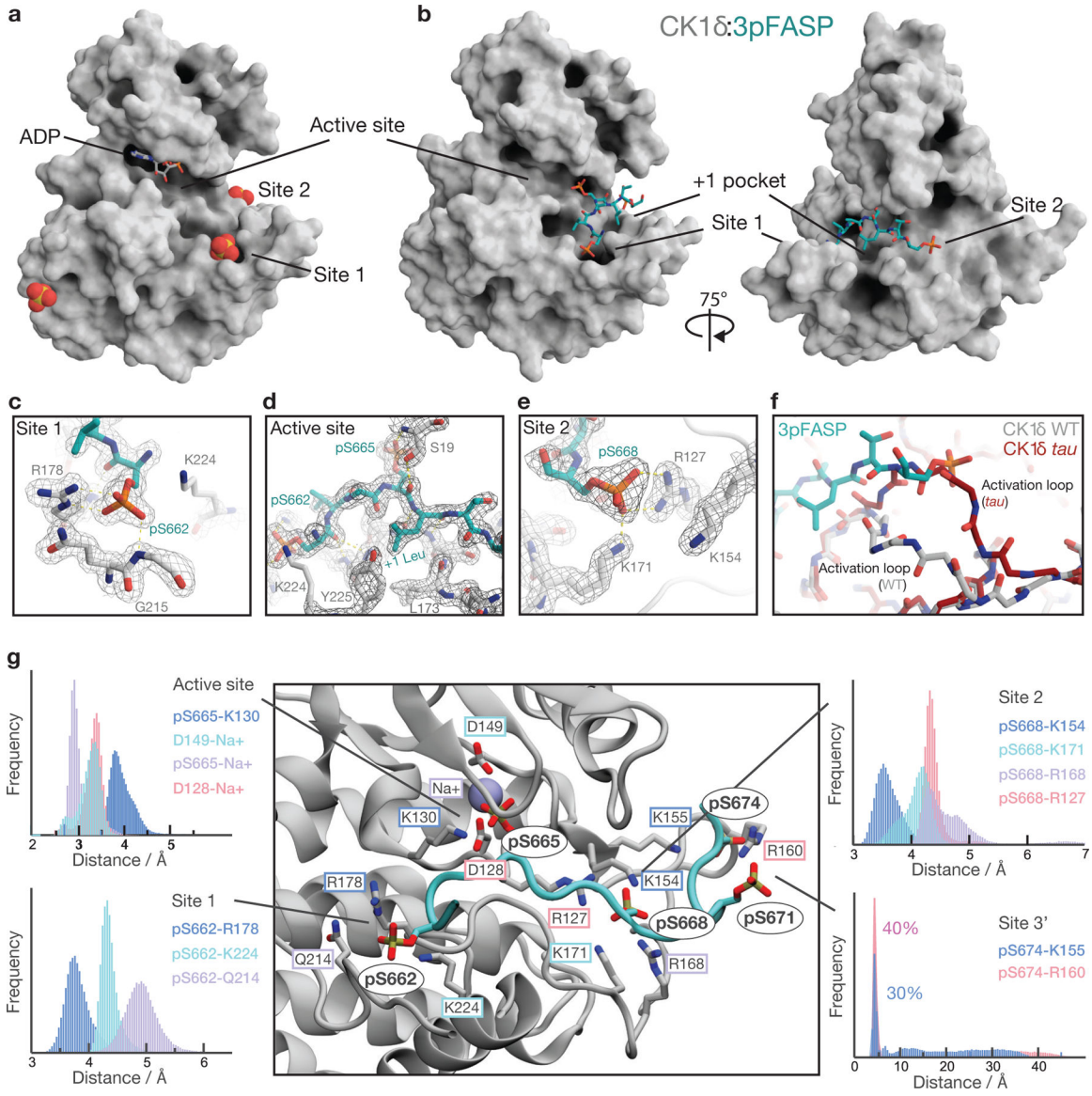


**Figure 4. The human PER2 pFASP binds to the active site of CK1.**

**a**, Surface representation of CK1 catalytic domain bound to ADP (PDB 5X17). Spheres, sulfate anions from the crystallization condition bound at anion binding sites as indicated. **b**, Surface representation of the CK1 catalytic domain bound to a human PER2 3pFASP peptide (see Supplementary Figure 3a). **c-e**, Zoom of 3pFASP interactions within anion binding site 1 (**c**), the active site (**d**), and anion binding site 2 (**e**). **f**, Structural alignment showing the main chain for the activation loop of CK1 WT (gray) and the *tau* mutant (red) showing a clash of the 3pFASP (teal) with the conformation of the activation loop stabilized by the *tau* mutation. **g**, Characterization of key interactions from molecular dynamics simulations that stabilize the 5pFASP product in the active site, Site 1, Site 2, and an additional anion binding site located proximal to Site 2 (Site 3'). Histograms were computed based on distances sampled during the GaMD simulations.

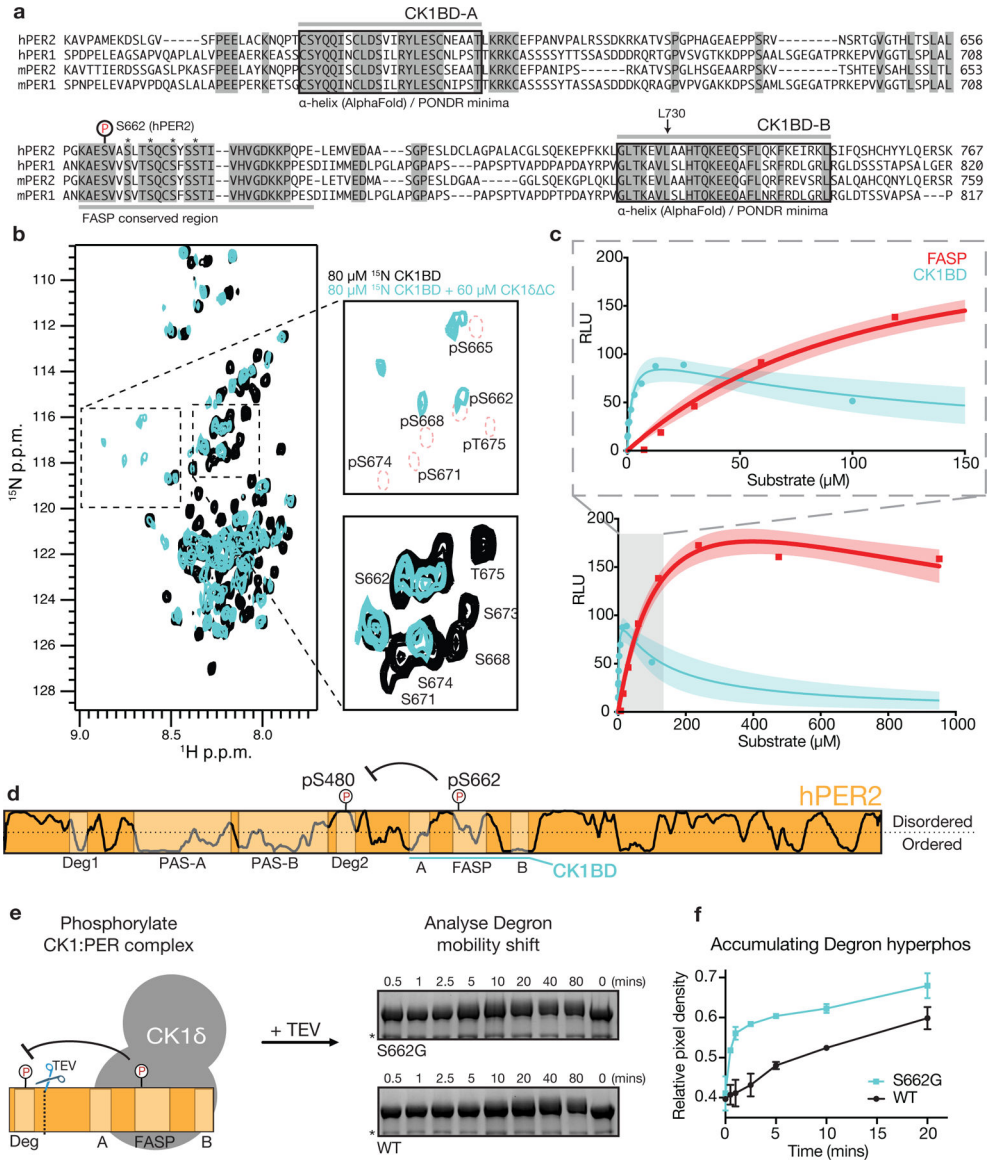


**Figure 5. Kinase anchoring interactions with the PER2 CK1BD increase FASP phosphorylation and feedback inhibition of CK1.**

**a**, Alignment of human and mouse PER1/2 proteins showing conservation of the disordered FASP region flanked by two highly conserved binding motifs (CK1BD-A/B) characterized as PONDR minima and predicted to be α-helices by AlphaFold2. The priming site (S662, human PER2 numbering) is shown, with sequential phosphorylation sites indicated by asterisks. **b**, $^{15}N/^{1}H$ HSQC of an engineered minimal CK1BD construct containing CK1BD-A, FASP, and CK1BD-B regions (residues 571–609, 645–687, 722–757) with (blue) and without CK1 (black). Upper zoom indicates the region corresponding to phosphoserines. Dashed red circles indicate the chemical shift of peaks corresponding to the 5 phosphoserines of the FASP peptide (see Figure 1b). Lower zoom indicates chemical shift environment of peaks corresponding to proximal residues in the FASP serine cluster. **c**, ADP-Glo kinase assay with titration of FASP peptide or CK1BD (residues 571–757) showing mean and SD from 2 replicates, representative of n = 3 independent assays.

Shaded area indicates 95% C.I. of the fit. Data were fit with a preferred substrate inhibition model. Zoom corresponds to the shaded grey area at lower substrate concentrations. **d**, Schematic representation of hPER2 depicting attenuation of Degron phosphorylation by the phosphorylated FASP region. **e**, Schematic representation of *in cis* phosphorylation assay using a CK1:PER2 complex (see methods). **f**, Densitometric quantification of the band corresponding to the hyperphosphorylated Degron.

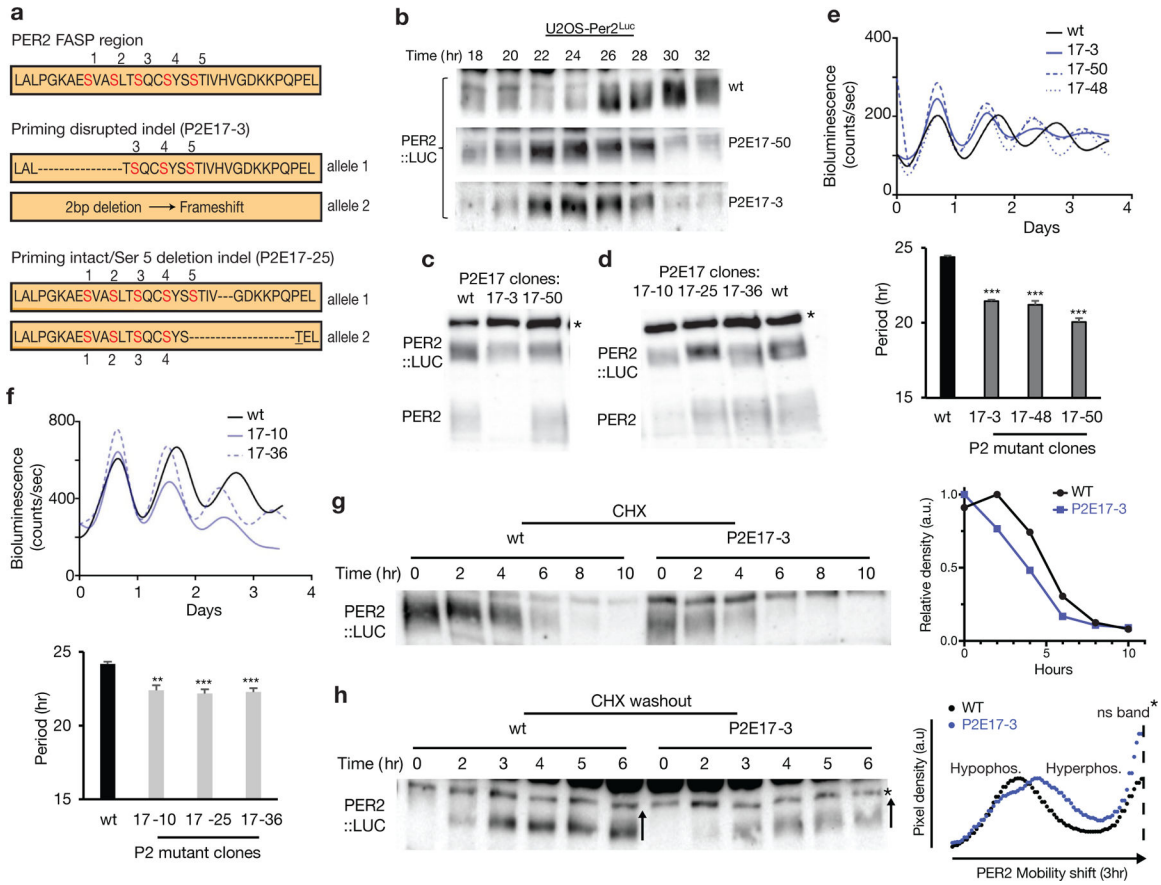


**Figure 6. Circadian rhythms are shortened by small deletions in the conserved FASP domain of human PER2.**

**a**, Schematic representation of select in-frame deletions within the human PER2 FASP region are separated into 2 classes: priming-disrupted (P2E17-3) or priming intact (P2E17-25). **b**, Immunoblot of select priming-disrupted PER2::LUC mutants compared to WT PER2::LUC. Blot representative of two independent experiments. **c**,**d**, Representative immunoblots for (**c**) priming-disrupted or (**d**) priming intact PER2 mutants. *nonspecific band. The *Per2* allele in clone 17–3 has a frame-shifting mutation leading to deletion of the untagged PER2. **e**,**f**, Real-time bioluminescence traces of circadian rhythms from WT and mutant *Per2* clones (**e**, priming-disrupted; **f**, priming intact) with quantification of mean period and SD from n = 3 cultures. Periods from mutant clones were compared to WT with an unpaired t-test: ***, $p < 0.001$. *Per2* priming intact mutants (clones 17–25 and 17–36) exhibited rhythms that were shortened to a lesser degree than the priming-disrupted mutants in **e**, $p < 0.05$. In both graphs, the first peaks are aligned to show differences in period clearly. **g**, Western blot and quantification of degradation of WT PER2::LUC and clone 17–3 after cycloheximide treatment. Blot representative of two independent assays (n = 2). **h**, Western blot and densitometric quantification of phosphorylation of *de novo* PER2 after protein depletion by 10 hr CHX treatment and washout. Blot representative of two independent assays (n = 2).

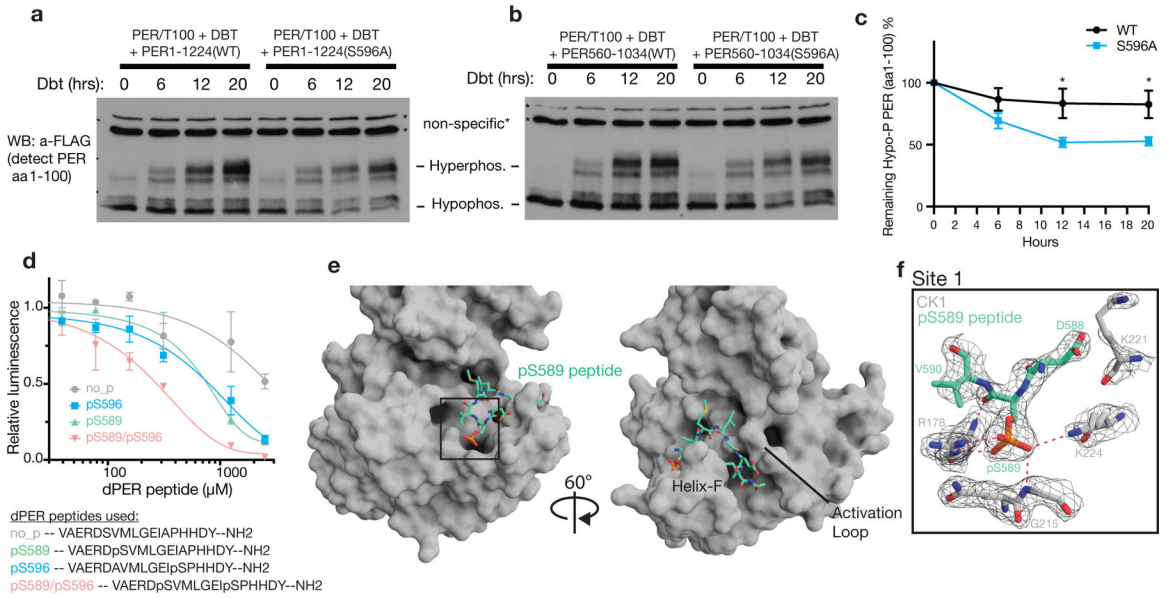


**Figure 7. The phosphorylated PER-Short domain of *Drosophila* PER binds CK1 Site 1 to inhibit kinase activity.**

**a-b,** Western blot of dPER fragment (aa1-100) cleaved from full-length dPER (**a**) or a fragment containing the dPER CK1BD but lacking the PAS dimerization domain (**b**) co-expressed with DBT. Samples collected at indicated timepoints after kinase induction, followed by protein extraction and TEV cleavage. **c**, Densitometric quantification of hypophosphorylated band (n = 4). WT and S596A compared with two-way ANOVA with Sidak multiple comparisons test: *, $p < 0.05$. **d**, ADP-Glo kinase assay of CK1 on the human PER2 PAS-Degron substrate in the presence of indicated peptides from dPER. Data are mean and SD from 2 replicates, representative of n = 3 independent assays. **e**, Structure of human CK1 (gray) bound to the dPER-Short peptide with pS589 (light green). **f**, Close-up view of dPER pS589 coordinated by CK1 residues in anion binding Site 1.

**Table 1.**

X-ray crystallography data collection and refinement statistics

| | 2pFASP:CK1δ | 3pFASP:CK1δ | 4pFASP:CK1δ | pS589:CK1δ |
|---|---|---|---|---|
| **Data collection** | | | | |
| PDB Id. | 8D7M | 8D7N | 8D7O | 8D7P |
| Beam line | APS(23IDD) | APS(23IDD) | APS(23IDD) | APS(23IDD) |
| Resolution Range (Å) (highest shell)* | 46.15 – 2.25 (2.32 – 2.25) | 68.01–1.66 (1.69 – 1.66) | 67.70 – 1.65 (1.68 – 1.65) | 60.77 – 2.25 (2.32 – 2.25) |
| Space group | C 1 2 1 | C 1 2 1 | C 1 2 1 | P1 |
| a, b, c | 55.7, 135.97, 91.14 | 55.90, 136.03, 90.54 | 55.33, 135.40, 90.35 | 48.78, 56.74, 65.94 |
| $\alpha, \beta, \gamma$ | 90, 94.3, 90 | 90, 94.60, 90 | 90, 94.41, 90 | 108.93, 95.63, 108.69 |
| Wavelength (Å) | 1.03 | 1.03 | 1.03 | 1.03 |
| Total observations | 176957 (15319) | 480416 (23861) | 468136 (24113) | 85303 (7506) |
| Unique reflections | 31319 (2767) | 79274 (3942) | 78946 (4059) | 27457 (2505) |
| Completeness (%) | 97.8 (94.5) | 100 (99.9) | 99.4 (99.2) | 93.7 (91.8) |
| $R_{merge}$ | 15.2 (127.4) | 9.3 (55.6) | 6.4 (54.2) | 11.6 (31.2) |
| $\langle I/\sigma \rangle$ | 9.4 (2.5) | 9.9 (2.7) | 13.6 (2.9) | 5.5 (2.7) |
| CC1/2 | 0.99 (0.55) | 0.99 (0.82) | 0.99 (0.84) | 0.98 (0.85) |
| Redundancy | 5.7 (5.5) | 6.1 (6.1) | 5.9 (5.9) | 3.1 (3.0) |
| **Refinement** | | | | |
| $R_{work}$/ $R_{free}$ (%) | 17.9 (22.9) | 18.8 (21.3) | 17.4 (21.1) | 19.7 (25.4) |
| Number of non-hydrogen atoms | 5075 | 5388 | 5342 | 4999 |
| Protein | 4820 | 4840 | 4840 | 4864 |
| Water | 255 | 548 | 502 | 135 |
| B-factor (Wilson) | 36.95 | 33.32 | 32.9 | 29.93 |
| RMSD Bond length (Å) | 0.008 | 0.01 | 0.011 | 0.009 |
| RMSD Bond angle | 1.05 | 1.18 | 1.18 | 1.04 |
| Ramachandran favored(%)/ Ramachandran outliers(%) | 97.04/0.0 | 96.17/0.0 | 96.34/0.26 | 96.23/0.0 |

## KEY RESOURCES TABLE

| REAGENT or RESOURCE | SOURCE | IDENTIFIER |
|---|---|---|
| Antibodies | | |
| anti-FLAG | Millipore Sigma | cat. # F1804 |
| anti-mouse IgG HRP | Millipore Sigma | cat. #12-349 |
| anti-PER1 | Lee et al., 2001 | GP62 |
| anti-PER2 | Lee et al., 2001 | GP49 |
| anti-guinea pig IgG HRP | Thermo Fisher Scientific | cat. # A18769 |
| anti-Myc agarose conjugate | Santa Cruz Biotechnology | cat. # sc-40 AC |
| α-Myc HRP | Santa Cruz Biotechnology | cat. # sc-40 HRP |
| α-OctA HRP | Santa Cruz Biotechnology | cat. # sc-166355 HRP |
| anti-Myc | Santa Cruz Biotechnology | cat. # sc-40 |
| Rabbit polyclonal phospho-Ser659 | Narasimamurthy et al., 2018 | N/A |
| anti-rabbit IgG HRP | Bio-Rad | cat. # 1706515 |
| anti-mouse IgG HRP | Bio-Rad | cat. # 1706516 |
| Bacterial and virus strains | | |
| *Escherichia coli* DH5a | NEB | cat. # C2987H |
| *Escherichia coli* BL21 (DE3) Rosetta2 | Fisher | cat. # 69041 |
| all-in-one CRISPR adenovirus | Jin YH et al., 2019 | N/A |
| Chemicals, peptides, and recombinant proteins | | |
| 2pFASP peptide | Biopeptide Co. | Lot #: 07102013610 |
| 3pFASP peptide | Biopeptide Co. | Lot #: 07102013611 |
| 4pFASP peptide | Biopeptide Co. | Lot #: 09082013881 |
| no_p peptide | Biopeptide Co. | Lot #: 11092115443 |
| pS589 peptide | Biopeptide Co. | Lot #: 11092115440 |
| pS596 peptide | Biopeptide Co. | Lot #: 11092115441 |
| pS589/pS596 peptide | Biopeptide Co. | Lot #: 11092115442 |
| HGS-CK1δ (1–294) | This study | N/A |
| HGST-CK1δ (1–317) | This study | N/A |
| HGST-CK1δ (1–317) K224D | This study | N/A |
| HNXL-PER1 FASP | This study | N/A |
| HNXL-PER1 FASP Indel P1E17-1 | This study | N/A |
| HNXL-PER1 FASP Indel P1E17-38 | This study | N/A |
| HNXL-PER2 FASP | This study | N/A |
| HNXL-PER2 FASP S662A | This study | N/A |
| HNXL-PER2 FASP S665A | This study | N/A |
| HNXL-PER2 FASP S668A | This study | N/A |
| HNXL-PER2 FASP S671A | This study | N/A |
| HNXL-PER2 FASP S674A | This study | N/A |

| REAGENT or RESOURCE | SOURCE | IDENTIFIER |
|---|---|---|
| HNXL-PER2 FASP S662D | This study | N/A |
| HNXL-PER2 PAS-Degron | This study | N/A |
| HNXL-PER2 CK1BD | This study | N/A |
| HNS-PER2 Degron-CK1BD-B TEV507 | This study | N/A |
| HNS-PER2 Degron-CK1BD-B TEV507 S662G | This study | N/A |
| His-TEV | Blommel et al., 2007 | N/A |
| Critical commercial assays | | |
| ADP-Glo | Promega | cat. # V9102 |
| Deposited data | | |
| Human FASP chemical shift assignments | This study | BMRB: 51827 |
| CK1δ:2pFASP structure | This study | PDB: 8D7M |
| CK1δ:3pFASP structure | This study | PDB: 8D7N |
| CK1δ:4pFASP structure | This study | PDB: 8D7O |
| CK1δ:pS589 structure | This study | PDB: 8D7P |
| Experimental models: Cell lines | | |
| Human: U2OS cells | ATCC | cat. # HTB-96 |
| Human: HEK293T cells | ATCC | cat. # CRL-3216 |
| *D. melanogaster*: S2 cells | Thermo Fisher Scientific | cat. # R69007 |
| Oligonucleotides | | |
| See Supplementary Table 4 | Millipore Sigma | N/A |
| Recombinant DNA | | |
| pET-22b(+) HGS-CK1δ (1–294) | This study | N/A |
| pET-22b(+) HGST-CK1δ (1–317) | This study | N/A |
| pET-22b(+) HGST-CK1δ K224D | This study | N/A |
| pET-22b(+) HNXL-PER2 FASP | This study | N/A |
| pET-22b(+) HNXL-PER2 FASP S662A | This study | N/A |
| pET-22b(+) HNXL-PER2 FASP S665A | This study | N/A |
| pET-22b(+) HNXL-PER2 FASP S668A | This study | N/A |
| pET-22b(+) HNXL-PER2 FASP S671A | This study | N/A |
| pET-22b(+) HNXL-PER2 FASP S674A | This study | N/A |
| pET-22b(+) HNXL-PER2 FASP S662D | This study | N/A |
| pET-22b(+) HNXL-PER2 PAS-Degron | This study | N/A |
| pET-22b(+) HNXL-PER2 CK1BD | This study | N/A |
| pET-22b(+) HNXL-PER1 FASP | This study | N/A |
| pET-22b(+) HNXL-PER1 FASP Indel P1E17-1 | This study | N/A |
| pET-22b(+) HNXL-PER1 FASP Indel P1E17-38 | This study | N/A |
| pAc-3XFLAG-His-d*per*/Tev100-6Xc-myc | Chiu et al., 2008 | N/A |
| pAc-d*per* WT (aa1-1224)-V5 | Chiu et al., 2011 | N/A |
| pAc-d*per* S596A (aa1-1224)-V5 | Chiu et al., 2011 | N/A |

| REAGENT or RESOURCE | SOURCE | IDENTIFIER |
|---|---|---|
| pAc-d*per* WT (aa560-1034)-V5 | Ko et al., 2010 | N/A |
| pCS MT-PER2 | This study | N/A |
| pCS MT-PER2 S662A | This study | N/A |
| pCS MT-PER2 S665A | This study | N/A |
| pCS MT-PER2 S668A | This study | N/A |
| pCS MT-PER2 S671A | This study | N/A |
| pCS MT-PER2 S674A | This study | N/A |
| pCS MT-PER2 S480A | This study | N/A |
| pcDNA4B-FLAG-CK1δ FLAG | This study | N/A |
| pcDNA4B-FLAG-CK1δ R178C (*tau*) FLAG | This study | N/A |
| pcDNA4B-β-TrCP | This study | N/A |
| all-in-one pAdTrack-Cas9-DEST | Jin YH et al., 2019 | N/A |
| Software and algorithms | | |
| PRISM | GraphPad | |
| Mathematica 11.0 | Wolfram Research | |
| ImageJ | NIH | 2.0.0-rc-67/1.52d |
| AMBER16 | Case, 2016 | |
| Maestro | Schrodinger | 2020-3 |
| PrepWizard | See method details | |
| PHENIX | Adams et al., 2011 | 1.13-2998 |
| Coot | CCP4 | 0.8.9.2 EL |
| PyMOL | Schrodinger LLC. | 2.1.1 |
| NMRPipe | Delaglio et al., 1995 | |
| CCPNmr Analysis | Vranken et al., 2005 | 2.5.2 |
| Excel | Microsoft | 16.61.1 |
| Other | | |
| | | |